

Permitted and restricted steps of human kinetochore assembly in mitotic cell extracts

Ekaterina V. Tarasovets^a, Praveen Kumar Allu^b, Robert T. Wimbish^c, Jennifer G. DeLuca^c,
Iain M. Cheeseman^d, Ben E. Black^{b,*}, and Ekaterina L. Grishchuk^{a,*}

^aDepartment of Physiology, Perelman School of Medicine, and ^bDepartment of Biochemistry and Biophysics, Penn Center for Genome Integrity, Epigenetics Institute, Perelman School of Medicine, University of Pennsylvania, Philadelphia, PA 19104; ^cDepartment of Biochemistry and Molecular Biology, Colorado State University, Fort Collins, CO 80523; ^dWhitehead Institute for Biomedical Research, Cambridge, MA 02142

ABSTRACT Mitotic kinetochores assemble via the hierarchical recruitment of numerous cytosolic components to the centromere region of each chromosome. However, how these orderly and localized interactions are achieved without spurious macromolecular assemblies forming from soluble kinetochore components in the cell cytosol remains poorly understood. We developed assembly assays to monitor the recruitment of green fluorescent protein-tagged recombinant proteins and native proteins from human cell extracts to inner kinetochore components immobilized on microbeads. In contrast to prior work in yeast and *Xenopus* egg extracts, we find that human mitotic cell extracts fail to support de novo assembly of microtubule-binding subcomplexes. A subset of interactions, such as those between CENP-A-containing nucleosomes and CENP-C, are permissive under these conditions. However, the subsequent phospho-dependent binding of the Mis12 complex is less efficient, whereas recruitment of the Ndc80 complex is blocked, leading to weak microtubule-binding activity of assembled particles. Using molecular variants of the Ndc80 complex, we show that auto-inhibition of native Ndc80 complex restricts its ability to bind to the CENP-T/W complex, whereas inhibition of the Ndc80 microtubule binding is driven by a different mechanism. Together, our work reveals regulatory mechanisms that guard against the spurious formation of cytosolic microtubule-binding kinetochore particles.

Monitoring Editor

Claire Walczak
Indiana University

Received: Jul 17, 2020

Revised: Apr 13, 2021

Accepted: Apr 26, 2021

This article was published online ahead of print in MBoC in Press (<http://www.molbiolcell.org/cgi/doi/10.1091/mbc.E20-07-0461>) on May 6, 2021.

Conflict of interest: The authors declare no competing interests.

Author contributions: E.V.T. performed all experiments on kinetochore assembly in vitro. P.K.A. reconstituted and characterized fluorescently labeled recombinant nucleosomes and generated the DLD-1 cell line expressing GFP-Dsn1-SD. I.M.C. provided recombinant CENP-T/W and the HeLa cell line expressing GFP-Dsn1-Δ91-113 and contributed to the design of the research. J.G.D. and R.T.W. provided recombinant full-length and Bronsai Ndc80 complexes. B.E.B., P.K.A., E.V.T., and E.L.G. devised experiments investigating the role of the nucleosome-dependent assembly pathway. E.V.T. and E.L.G. designed the research project, analyzed the data, and wrote the paper with input from B.E.B., I.M.C., J.G.D., P.K.A., and R.T.W.

*Address correspondence to: Ekaterina L. Grishchuk (gekate@penmedicine.upenn.edu) and Ben E. Black (blackbe@penmedicine.upenn.edu).

Abbreviations used: BSA, bovine serum albumin; CCAN, constitutive centromere-associated network; CENP, centromere protein; DIC, differential interference contrast; DTT, dithiothreitol; EGTA, ethylene glycol tetraacetic acid; GFP, green fluorescent protein; PBS, phosphate-buffered saline; TIRF, total internal reflection fluorescence; YFP, yellow fluorescent protein.

© 2021 Tarasovets *et al.* This article is distributed by The American Society for Cell Biology under license from the author(s). Two months after publication it is available to the public under an Attribution–Noncommercial–Share Alike 3.0 Unported Creative Commons License (<http://creativecommons.org/licenses/by-nc-sa/3.0/>).

“ASCB®,” “The American Society for Cell Biology®,” and “Molecular Biology of the Cell®” are registered trademarks of The American Society for Cell Biology.

INTRODUCTION

Accurate chromosome segregation depends on proper interactions between spindle microtubules and the kinetochore, a multiprotein complex located at each centromere. Kinetochore assembly is a complex process, requiring the execution of multiple binding reactions in an ordered and localized manner (Cheeseman, 2014; Nagpal and Fukagawa, 2016; Musacchio and Desai, 2017). Kinetochore assembly is nucleated by inner kinetochore proteins localized at the centromere, which is marked by nucleosomes containing centromere protein A (CENP-A) (Fukagawa and Earnshaw, 2014; McKinley and Cheeseman, 2016). At the onset of mitosis, the CENP-A nucleosomes and proteins of the constitutive centromere-associated network (CCAN) recruit multiple copies of outer kinetochore proteins from their soluble pools (Figure 1A). Among them are the Ndc80 complex, Mis12 complex, and Knl1 protein, constituting the KMN network that links centromeres and spindle microtubules (Cheeseman, 2014; Nagpal and Fukagawa, 2016; Musacchio and Desai, 2017). The four-subunit Ndc80 complex is the major microtubule-binding component of the kinetochore (reviewed in Cheeseman *et al.*, 2006; Musacchio and Desai, 2017).

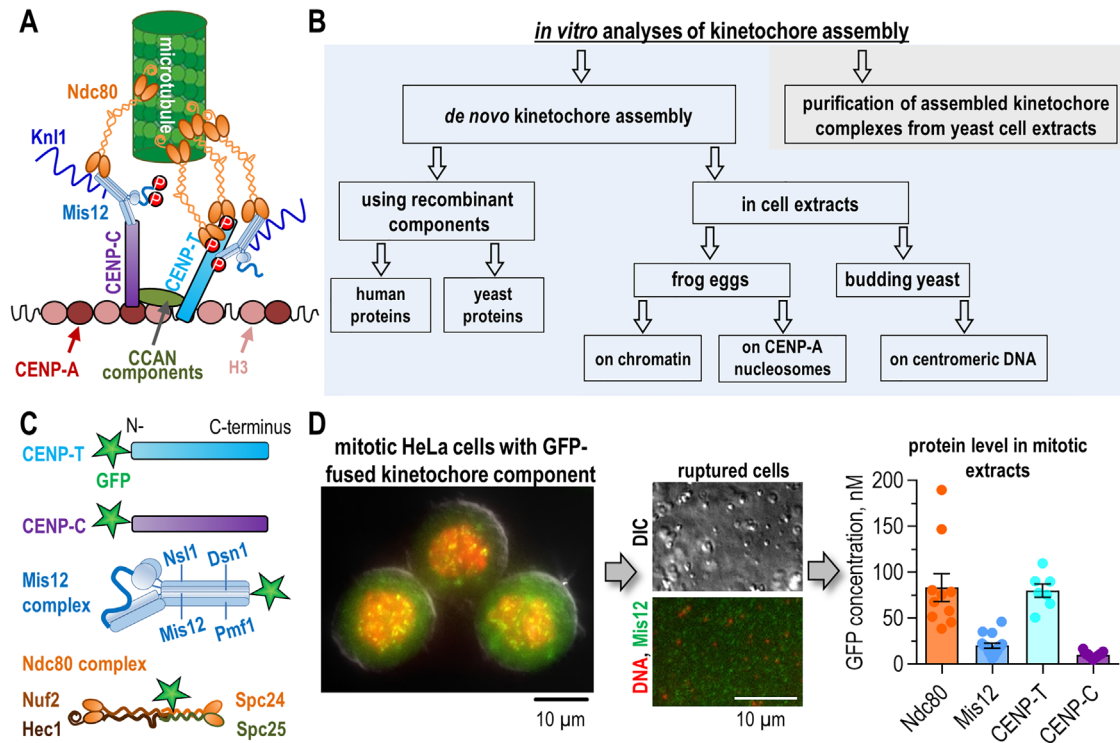


FIGURE 1: Strategies for reconstructing kinetochores and our experimental approach. (A) Principal architecture of mitotic kinetochore and its binding to microtubules; see the text for details. CCAN, constitutive centromere-associated network. Letters “P” on CENP-T indicate phosphorylation-dependent activation of its binding to Ndc80 and Mis12 complexes; letters “P” on Mis12 indicate phosphorylation-dependent activation of its binding to CENP-C. (B) Previous experimental approaches to reconstitute kinetochore assembly and function *in vitro*; see the text for references. (C) Schematic of GFP-fused proteins stably expressed in HeLa cells. Experiments with Ndc80 complexes used three different cell lines: Nuf2-GFP (shown), GFP-Spc24, and GFP-Spc25. (D) Key steps of our experimental approach. Left image shows representative HeLa cell that was fixed and stained with propidium iodide to reveal DNA; green signal is from Mis12-GFP. Graph shows concentration of GFP-fused kinetochore proteins in cell extracts. Each colored point represents average bead brightness from independent experiments, during which 50–100 beads were analyzed. For more detailed statistics, see the Supplemental Source data. Black lines show mean with SEM. The column for native Ndc80-GFP combines data from cell lines expressing GFP-fused Nuf2, Spc24, and Spc25.

In human cells, two major molecular scaffolds tether the KMN network to kinetochores: the constitutive inner kinetochore components CENP-T and CENP-C (Figure 1A) (Gascoigne *et al.*, 2011; Kim and Yu, 2015; Rago *et al.*, 2015; Suzuki *et al.*, 2015; Huis In ‘t Veld *et al.*, 2016). Work in multiple systems suggests that these assembly steps are regulated by mitotic kinases. The C-terminus of CENP-T, in complex with CENP-W, -S, and -X, is anchored directly to the centromeric DNA (Hori *et al.*, 2008; Nishino *et al.*, 2012), whereas the N-terminus of CENP-T recruits one Ndc80 via the Mis12 complex. *In vitro* reconstructions using high concentration of soluble proteins show that the CENP-T N-terminus can additionally bind to two Ndc80 complexes by direct interaction with the Spc24/25 subunits (Huis In ‘t Veld *et al.*, 2016). All of these interactions are promoted by phosphorylation of the CENP-T N-terminus by CDK1 kinase (Nishino *et al.*, 2013; Rago *et al.*, 2015; Huis In ‘t Veld *et al.*, 2016), which is distributed ubiquitously in mitotic cytoplasm and can presumably activate the entire pool of soluble and kinetochore-localized CENP-T.

KMN complex recruitment via CENP-C, which is anchored at the CENP-A nucleosomes (Carroll *et al.*, 2010; Kato *et al.*, 2013; Guo *et al.*, 2017; Watanabe *et al.*, 2019), is also regulated by phosphorylation, but these regulatory interactions may be more local. The N-terminus of CENP-C has one Mis12-binding site (Petrovic *et al.*, 2016), but these interactions are impeded because the N-terminal

tail of the Dsn1 subunit of Mis12 complex masks its CENP-C-binding site. Aurora B kinase, presumably in the kinetochore-bound form, phosphorylates the Dsn1 N-tail, thereby relieving this auto-inhibition (Yang *et al.*, 2008; Kim and Yu, 2015; Rago *et al.*, 2015; Petrovic *et al.*, 2016; Bonner *et al.*, 2019). An additional regulatory mechanism that ensures interaction only between the kinetochore-bound forms of CENP-C and Mis12 is found in yeast, where auto-inhibition of CENP-C is relieved by its anchoring at CENP-A nucleosome (Killinger *et al.*, 2020). Thus, some kinetochore assembly steps may require binding to the already assembled kinetochore structure or in proximity to regulatory kinases.

Yet another regulatory step in the formation of functional kinetochore involves activation of the microtubule binding of the Ndc80 complex. Work *in vitro* shows that soluble yeast Ndc80 complexes have reduced microtubule binding due to intramolecular inhibition (Kudalkar *et al.*, 2015; Scarborough *et al.*, 2019). Binding between the Spc24/Spc25 subunits of the Ndc80 complex and the C-termini of the Dsn1 and Nsl1 subunits of the Mis12 complex (Petrovic *et al.*, 2010, 2016) alleviates the intramolecular inhibition of Ndc80 (Kudalkar *et al.*, 2015; Scarborough *et al.*, 2019), enabling formation of kinetochore subcomplexes with enhanced microtubule-binding affinity. It is presently unknown whether these interactions are restricted to the centromeric regions or they can also take place in the cytosol of mitotic cells.

The molecular and structural cues that orchestrate the hierarchical assembly of all these components, and how these interactions are regulated in cytosol versus at the maturing kinetochore, remain incompletely understood. In recent years, significant progress in dissecting these interactions has been achieved using artificial tethering of inner kinetochore components to Lac operator repeats integrated at noncentromeric regions in human and chicken cells (reviewed in Hori and Fukagawa, 2020). Expression of the LacI fusion with the CENP-A–specific chaperone HJURP induces formation of ectopic kinetochore loci (Barnhart *et al.*, 2011). Moreover, similar tethering of the N-terminal fragments of either CENP-T or CENP-C is also sufficient to cause local kinetochore assembly (Gascoigne *et al.*, 2011; Hori *et al.*, 2013; Rago *et al.*, 2015). The rapid assembly of the outer kinetochore from the cytosolic pool of kinetochore components upon mitotic entry (Gascoigne and Cheeseman, 2013) strongly suggests that soluble components are fully competent to assemble the microtubule-binding structures. However, these soluble binding reactions appear to be restricted, requiring nucleation by clusters of inner kinetochore scaffolds.

By contrast, recombinant kinetochore proteins can readily assemble *in vitro*, as demonstrated by the tour-de-force studies that assembled the entire linkage between human CENP-A nucleosomes, inner kinetochore components, and KMN (Figure 1B) (Weir *et al.*, 2016; Pesenti *et al.*, 2018). A recent study using recombinant *Saccharomyces cerevisiae* proteins demonstrated that 14 CCAN subunits have the ability to self-assemble in the presence of CENP-A nucleosomes (Yan *et al.*, 2019). Another study with recombinant yeast proteins revealed self-assembly of protein chains consisting of CENP-A nucleosomes, CENP-C and CENP-QU (Okp1/Ame1 complex) scaffolds, and the Mis12 and Ndc80 complexes (Hamilton *et al.*, 2020). These reconstituted chains bind to polymerizing microtubule ends and rupture under forces in the 4–8 pN range. Thus, recombinant kinetochore proteins lacking posttranslational modifications or bearing specific phosphomimetic substitutions appear to have a strong propensity to self-assemble *in vitro*.

Prior work has also analyzed kinetochore formation in cell extracts, which provide a rich source of kinetochore proteins with natural posttranslational modifications (Sorger *et al.*, 1994; Desai *et al.*, 1997; De Wulf *et al.*, 2003; Emanuele *et al.*, 2005; Akiyoshi *et al.*, 2010; Guse *et al.*, 2011; Krizaic *et al.*, 2015; Bonner *et al.*, 2019). In *Xenopus* egg extracts, soluble kinetochore components, including CENP-C, CENP-T, and KMN, have been successfully recruited using sperm chromatin (Krizaic *et al.*, 2015; Haase *et al.*, 2017; Bonner *et al.*, 2019) or CENP-A nucleosome arrays (Guse *et al.*, 2011). The reconstructed assemblies exhibit microtubule binding and spindle checkpoint activities (Desai *et al.*, 1997; Emanuele *et al.*, 2005; Guse *et al.*, 2011; Haase *et al.*, 2017). Importantly, the successful assembly of kinetochore components in this system requires a critical regulatory step—phosphorylation of the Dsn1 subunit by Aurora B kinase (Haase *et al.*, 2017; Bonner *et al.*, 2019). Indeed, the Mis12 complex containing phosphomimetic substitutions in Dsn1 (S77E, S84E) allows robust assembly of functional kinetochores in *Xenopus* egg extracts even if Aurora B is inhibited (Bonner *et al.*, 2019). In yeast cell extracts, multicomponent kinetochore complexes can be assembled *de novo* using centromeric DNAs as templates (Sorger *et al.*, 1994; Sandall *et al.*, 2006; Lang *et al.*, 2018). In this system, recruitment of KMN components was possible in the absence of Dsn1 phosphorylation, although assembly increased up to sevenfold in extracts from cells with phosphomimetic mutations in Dsn1 (S240D, S250D).

Interestingly, isolation of the Mis12 complex from yeast extracts yields macromolecular complexes that are highly enriched in other

kinetochore proteins (De Wulf *et al.*, 2003) and even represent intact kinetochore “particles” that exhibit microtubule binding (Akiyoshi *et al.*, 2010; Gupta *et al.*, 2018) (Figure 1B). Load-bearing and microtubule tip-tracking by these particles is significantly more robust than what is seen with recombinant Ndc80 complexes alone (Powers *et al.*, 2009; Akiyoshi *et al.*, 2010). It remains unknown whether cell extracts from mitotic human cells contain analogous functionally active kinetochore complexes. In dividing cells, cytosolic pools of green fluorescent protein (GFP)-tagged kinetochore components fail to bind to spindle microtubules and remain soluble even when overexpressed, suggesting that binding reactions between some or all soluble kinetochore proteins may be restricted. However, which steps in kinetochore assembly are regulated in this manner has not been investigated systematically. Here, we use microscopy-based *in vitro* reconstruction approaches to analyze kinetochore assembly pathways and the microtubule-binding activity of native kinetochore proteins in extracts prepared from mitotic human cells.

RESULTS

Kinetochore complexes in human mitotic cell extracts bind microtubules with low affinity

To directly investigate the microtubule-binding activity of kinetochore complexes found in the cytoplasm of mitotic human cells, we developed a minimally invasive protocol to prepare cytosolic fractions with fluorescently labeled kinetochore proteins. To this end, HeLa cells stably expressing GFP fusions of individual components of the Mis12 complex, Ndc80 complex, CENP-T, or CENP-C, were arrested in mitosis with nocodazole (Figure 1C). The arrested cells were lysed and ruptured by gentle sonication, and the solution was clarified by centrifugation to obtain mitotic cell extracts. The concentrations of GFP-tagged kinetochore proteins in the extracts were in the 10–100 nM range (Figure 1D), consistent with protein levels for these components determined by previous studies (Supplemental Table 1) (Itzhak *et al.*, 2016; Cai *et al.*, 2018).

Using total internal reflection fluorescence (TIRF) microscopy, we visualized binding of these native kinetochore complexes to fluorescently labeled microtubules stabilized with the nonhydrolyzable GTP analogue GMPCPP (Figure 2, A–C). Ndc80-GFP complexes exhibited frequent microtubule-binding events, but they were not as robust as those observed for bacterially purified “Bronsai” Ndc80 complex, a shortened version of Ndc80 complex with wild-type microtubule-binding domains (Supplemental Figure 1) (Wimbish *et al.*, 2020). Microtubule binding by Bronsai Ndc80 was reduced when these interactions were examined in the presence of control cell extracts containing no GFP-tagged proteins (Figure 2, B and C; Supplemental Figure 1), probably owing to the nonspecific blocking or competition with other microtubule-binding proteins in cell extracts. However, even under these conditions, recombinant Bronsai Ndc80 complex was fourfold more active than the native Ndc80 complex, suggesting that the differences in microtubule binding between these proteins is caused by differences in their molecular structures or posttranslational modifications, rather than the presence of other cytoplasmic proteins. Similarly poor binding was observed for native Ndc80 complexes in which GFP was fused to the Nuf2, Spc24, or Spc25 subunits, indicating that the partial inhibition was not caused by the tag location.

The interaction of the Ndc80 complex with other soluble kinetochore components may promote its microtubule-binding activity (Cheeseman *et al.*, 2006; Kudalkar *et al.*, 2015; Scarborough *et al.*, 2019). We therefore tested the microtubule binding of native complexes visualized via the GFP-labeled CENP-T,

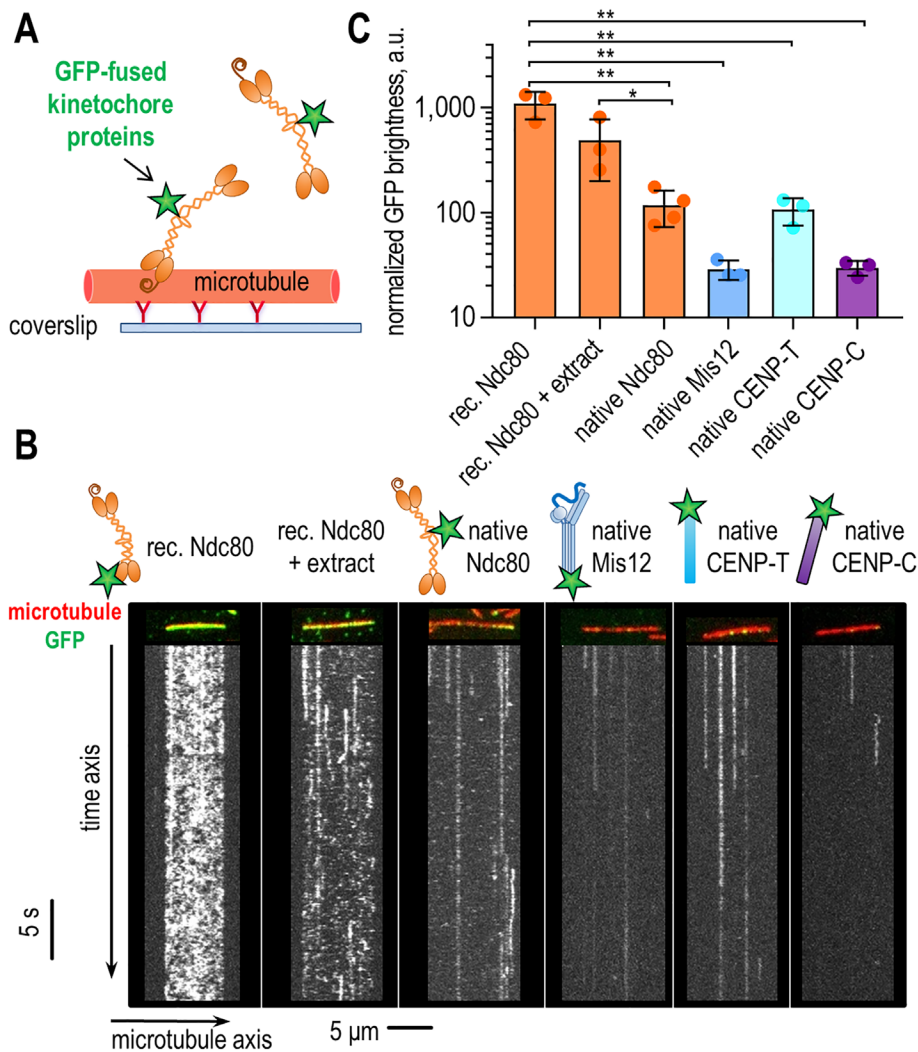


FIGURE 2: Microtubule binding by native kinetochore complexes in mitotic cell extracts. (A) Scheme of TIRF-based assay to visualize binding of soluble GFP-fused kinetochore components (2.5–3 nM) to GMPCPP-stabilized and fluorescently labeled microtubules, which were immobilized on the coverslip via anti-tubulin antibodies. (B) Colored images show representative microtubules (red) with bound GFP-fused kinetochore complexes (green); the corresponding grayscale kymographs below reveal mobility of these complexes over 30-s observation time; “rec” correspondents to purified recombinant proteins. (C) Average GFP brightness of microtubule decoration normalized against the concentration of GFP-labeled kinetochore protein (means with SD); note semi-log scale. Each point represents an independent experiment in which brightness was collected from >18 microtubules. *p* values were calculated by unpaired *t* test: *, *p* < 0.05; **, *p* < 0.01. For more detailed statistics, see the Supplemental Source data.

CENP-C, and Mis12 components. We detected some binding events between the GFP-labeled complexes and stabilized microtubules. These associations lasted visibly longer than those seen for native Ndc80-containing complexes, but they were much less frequent, indicating strong molecular heterogeneity (Figure 2, B and C). Because CENP-T, CENP-C, and Mis12 complex do not have significant microtubule-binding activity on their own, these observations suggest that only a small fraction of cytosolic complexes is associated with microtubule-binding proteins, such as the Ndc80 complex. Another possible explanation for these results is that native Ndc80 readily forms complexes with other soluble kinetochore proteins, but its microtubule-binding activity is reduced.

and bead-bound) is auto-inhibited, whereas recombinant Bronsai construct is active due to its truncated stalk. To investigate, we expressed and purified full-length human Ndc80 complex from insect cells. Unexpectedly, its microtubule-binding activity *in vitro* was more similar to that of Bronsai Ndc80 than that of the native full-length Ndc80 complex (Figure 3, B–D). Thus, different microtubule-binding behaviors observed for the native and recombinant Ndc80 complexes cannot be explained by their different molecular structures.

Because recruitment of yeast Ndc80 complex to Mis12 increases the affinity of Ndc80 for microtubules *in vitro* (Kudalkar *et al.*, 2015; Scarborough *et al.*, 2019), we expected that Mis12-GFP complexes conjugated to the bead surface would exhibit improved microtubule

Native Ndc80 complex is inhibited for both microtubule binding and assembly with other kinetochore components

To gain insights into the mechanisms that prevent the formation of microtubule-binding kinetochore complexes in human cell extracts, we examined the activity of these proteins conjugated to microbeads. This configuration provides more physiological molecular arrangement for kinetochore proteins and could serve to activate kinetochore proteins by suppressing auto-inhibitory mechanisms, as seen for microtubule motors (Coy *et al.*, 1999; Gudimchuk *et al.*, 2013). After conjugation of kinetochore proteins via the GFP tag, the beads were washed to remove unbound cytosolic proteins and incubated with fluorescently labeled stabilized microtubules (Figure 3, A and B).

As a positive control, we used beads coated with recombinant Bronsai, which readily recruited microtubules to the bead surface, as observed previously for other recombinant Ndc80 complexes (McIntosh *et al.*, 2008; Powers *et al.*, 2009; Chakraborty *et al.*, 2019; Wimbish *et al.*, 2020). As an additional control, we coated beads with Bronsai Ndc80 complexes in the presence of unlabeled cell extracts followed by washing. Incubation with cell extract did not alter the microtubule binding of these beads, consistent with our conclusion from the TIRF-based assay that these interactions are largely driven by the Ndc80 proteins rather than other cytosolic factors (Figure 3, C and D).

Using this assay, we found that bead-bound clusters of native Ndc80 complexes interacted with microtubules less strongly than Bronsai Ndc80 (Figure 3, B–D), indicating that clustering native Ndc80 complexes on microbeads does not promote their full activation. On the basis of work with yeast Ndc80 complex, which is auto-inhibited for microtubule binding (Kudalkar *et al.*, 2015; Scarborough *et al.*, 2019), we hypothesized that human native Ndc80 protein (soluble

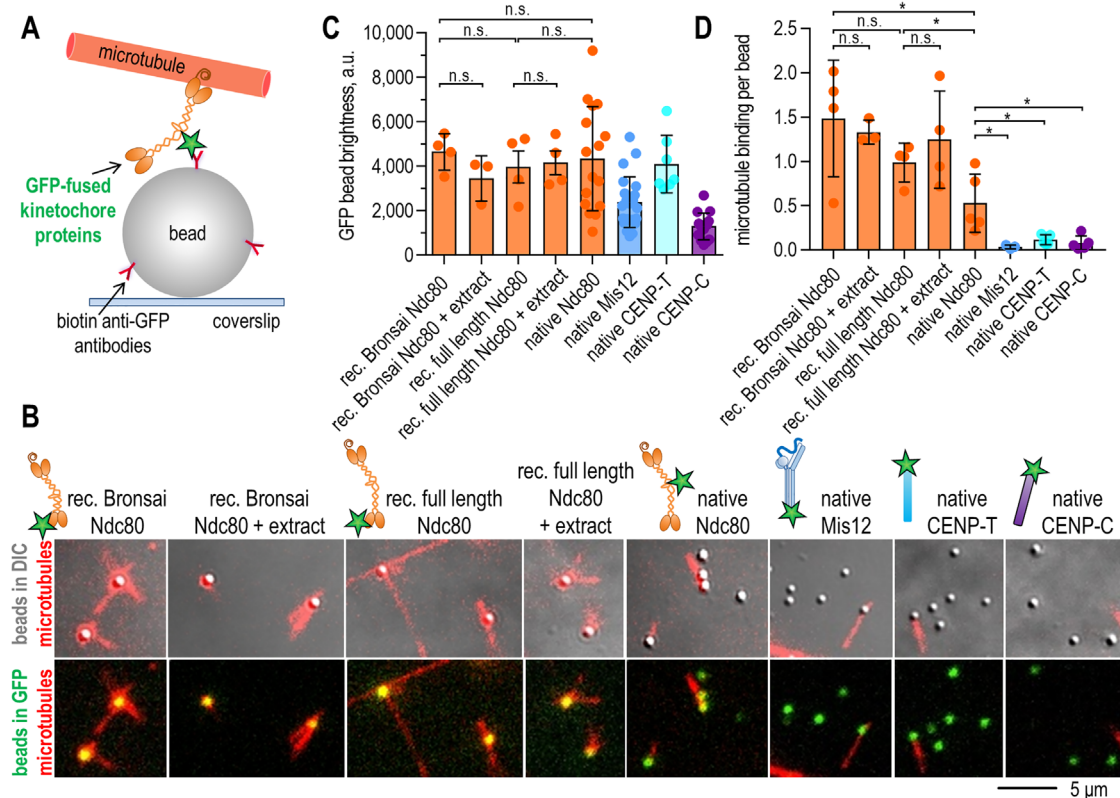


FIGURE 3: Microtubule binding by native kinetochore complexes clustered on microbeads. (A) Scheme of bead-based assay to test microtubule binding of kinetochore components. (B) Representative examples of microscopy fields showing microtubules (red) and GFP-fused kinetochore components conjugated to coverslip-immobilized beads, shown in the DIC (top) and GFP (bottom) channels. (C) Average GFP bead brightness corresponding to the coating density of GFP-fused kinetochore components on bead surfaces. Identical quantification procedures were used throughout this study, so GFP-bead brightness can be compared directly between different panels and graphs. (D) Average number of bead-bound microtubules normalized against the number of beads per imaging field. In panels C and D, means are shown with SD, and each point represents an independent experiment. *p* values were calculated by unpaired *t* test: n.s., *p* > 0.05; *, *p* < 0.05. For more detailed statistics, see the Supplemental Source data. Results for native Ndc80-GFP combine data from cell lines expressing GFP-fused Nuf2, Spc24, and Spc25.

binding relative to native Ndc80 complexes alone. However, microtubule binding by clusters of human native Mis12-GFP was even poorer. This result is in striking contrast to the behavior of yeast Mis12-containing complexes, which exhibit durable microtubule associations (Akiyoshi *et al.*, 2010). Bead-bound human CENP-T and CENP-C complexes had similarly low microtubule-binding activity (Figure 3), as seen with soluble complexes. To directly test whether native Ndc80 complexes were successfully recruited to these beads but remained inactive, we used immunostaining. We observed that native CENP-T or Mis12 had very little associated Ndc80 protein (Supplemental Figure 3). Thus, extracts prepared from mitotic human cells have virtually no Ndc80-containing preassembled kinetochore complexes, whereas the microtubule-binding activity of the Ndc80 protein is strongly reduced, explaining the absence of active kinetochore particles in human cell extracts.

In mitotic cell extracts, recruitment of Ndc80 complexes via the CENP-T pathway is blocked

We next investigated whether recruitment of outer kinetochore proteins can be triggered using inner kinetochore components as nucleators for the assembly reactions. First, we purified full-length CENP-T/W complex, which has previously been shown to bind directly to the Ndc80 and Mis12 complexes (Gascoigne *et al.*, 2011; Gascoigne and Cheeseman, 2013; Nishino *et al.*, 2013; Kim and Yu,

2015; Rago *et al.*, 2015; Huis In 't Veld *et al.*, 2016). We clustered CENP-T/W on beads via anti-CENP-T antibodies and incubated these beads with recombinant Bonsai Ndc80, a shortened Ndc80 complex that contains the kinetochore targeting domains formed by Spc24/25 subunits (Figure 4A). As expected, the CENP-T/W complex recruited Bonsai Ndc80 (Nishino *et al.*, 2013), but not Broccoli Ndc80 complex, which lacks the Spc24/25 subunits (Schmidt *et al.*, 2012). Moreover, Bonsai Ndc80 binding was enhanced when we used a version of the CENP-T/W complex containing three phosphomimetic substitutions in the CDK target sites (T11D, T27D, and T85D; Figure 4, B and C), which are known to promote Ndc80 binding (Nishino *et al.*, 2013; Huis In 't Veld *et al.*, 2016; Hara *et al.*, 2018). These phosphomimetic substitutions were not sufficient to promote recruitment of native Mis12-GFP from cell extracts, consistent with the requirement for additional phosphorylation in positions T195 and S201 (Rago *et al.*, 2015; Huis In 't Veld *et al.*, 2016).

Binding of native Ndc80 to CENP-T/W beads was then examined using human mitotic cell extracts containing GFP-tagged Ndc80 complex at a concentration similar to that of the recombinant Ndc80 proteins. Strikingly, native Ndc80 failed to be recruited by recombinant CENP-T/W protein, and no enhancement was detected with the phosphomimetic CENP-T/W complex (Figure 4, B and C). To gain insights into the underlying mechanisms for this inhibition, we used recombinant full-length Ndc80 complex. Full-length

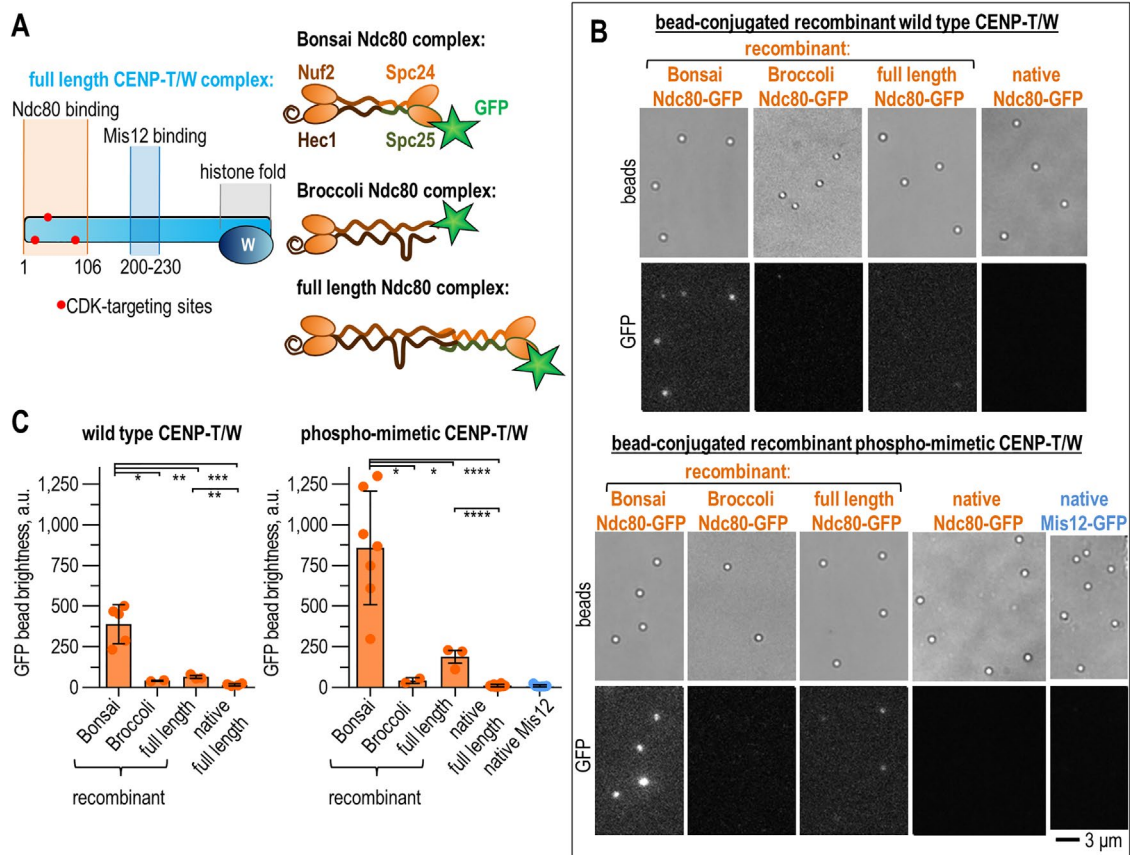


FIGURE 4: Interactions between various Ndc80 complexes and recombinant CENP-T/W complex. (A) Schematic representation of recombinant CENP-T/W protein, which serves as inner kinetochore scaffold. The phosphomimetic substitutions in CENP-T/W are indicated by red dots (left). Schematic representation of recombinant Ndc80 constructs (right). (B) Representative images of coverslip-immobilized beads in bright-field and GFP channels, showing recruitment of GFP-fused Ndc80 complexes to recombinant wild-type (top) or phosphomimetic (bottom) CENP-T/W, which has no fluorescent tag. (C) Average GFP bead brightness (mean with SD) of wild-type (left) or phosphomimetic (right) CENP-T/W-coated beads incubated with various Ndc80 (orange) or Mis12 (blue) proteins, as in panel B. Each point is derived from an independent experiment and represents the average brightness of >30 beads. p values were calculated by unpaired t test: *, $p < 0.05$; **, $p < 0.01$; ***, $p < 0.001$; ****, $p < 0.0001$. For more detailed statistics, see the Supplemental Source data. Concentrations of GFP-labeled soluble proteins, applied as minimally diluted mitotic cell extracts, were as follows: 50–190 nM Ndc80 and 10–80 nM Mis12 complexes. Recombinant proteins were used at 100–130 nM.

recombinant Ndc80 also failed to bind to CENP-T/W beads, behaving similarly to native Ndc80 complexes rather than other Ndc80 recombinant proteins. However, recruitment of recombinant full-length Ndc80 was enhanced by coating beads with phosphomimetic CENP-T/W protein, in agreement with prior studies using high concentrations of soluble proteins (5–12 μ M) (Huis In 't Veld *et al.*, 2016). Thus, our using physiological concentrations of recombinant Ndc80 complexes (~100 nM) revealed that binding of full-length Ndc80 to phosphomimetic CENP-T/W is significantly weaker than binding by Bonsai Ndc80 protein. This result strongly suggests that full-length Ndc80 complex is auto-inhibited for CENP-T binding. However, because recombinant full-length Ndc80 complex binds to CENP-T/W beads significantly better than the native Ndc80 complex, auto-inhibition alone cannot explain the lack of interaction between native Ndc80 and CENP-T proteins in human mitotic extracts.

Recombinant CENP-A nucleosomes bind native CENP-C, but outer kinetochore complexes are not recruited

Next, we investigated whether formation of functional complexes could be triggered using centromere-specific CENP-A nucleosomes as templates. We reconstituted recombinant CENP-A nucleosomes (Sekulic and Black, 2016; Allu *et al.*, 2019) using a Cy5-labeled 147-base-pair sequence that corresponds to the preferred assembly site within a monomer of repetitive human centromeric α -satellite DNA (Hasson *et al.*, 2013; Falk *et al.*, 2015) (Figure 5, A–C). Nucleosomes were immobilized at the surface of the antibody-coated beads via a His-tag engineered at the N-terminus of H2A histone (Figure 5D). Successful conjugation of these and similarly prepared H3 nucleosomes, which served as a negative control, was confirmed via Cy5 fluorescence. Cell extract prepared from mitotic HeLa cells stably expressing GFP-fused CENP-C was incubated with the nucleosome-coated beads. GFP-CENP-C bound to beads with CENP-A nucleosomes (Figure 5, E and F), consistent with the direct nature of this interaction (Carroll *et al.*, 2010; Kato *et al.*, 2013; Falk *et al.* 2015, 2016). These interactions were specific because canonical H3 nucleosomes did not recruit CENP-C. The level of CENP-C recruitment to CENP-A-coated beads was likely to be higher than what was detected with GFP fluorescence, because both GFP-tagged and untagged CENP-C proteins could bind to these nucleosomes. CENP-C enrichment on the beads was also observed using extracts prepared from DLD-1

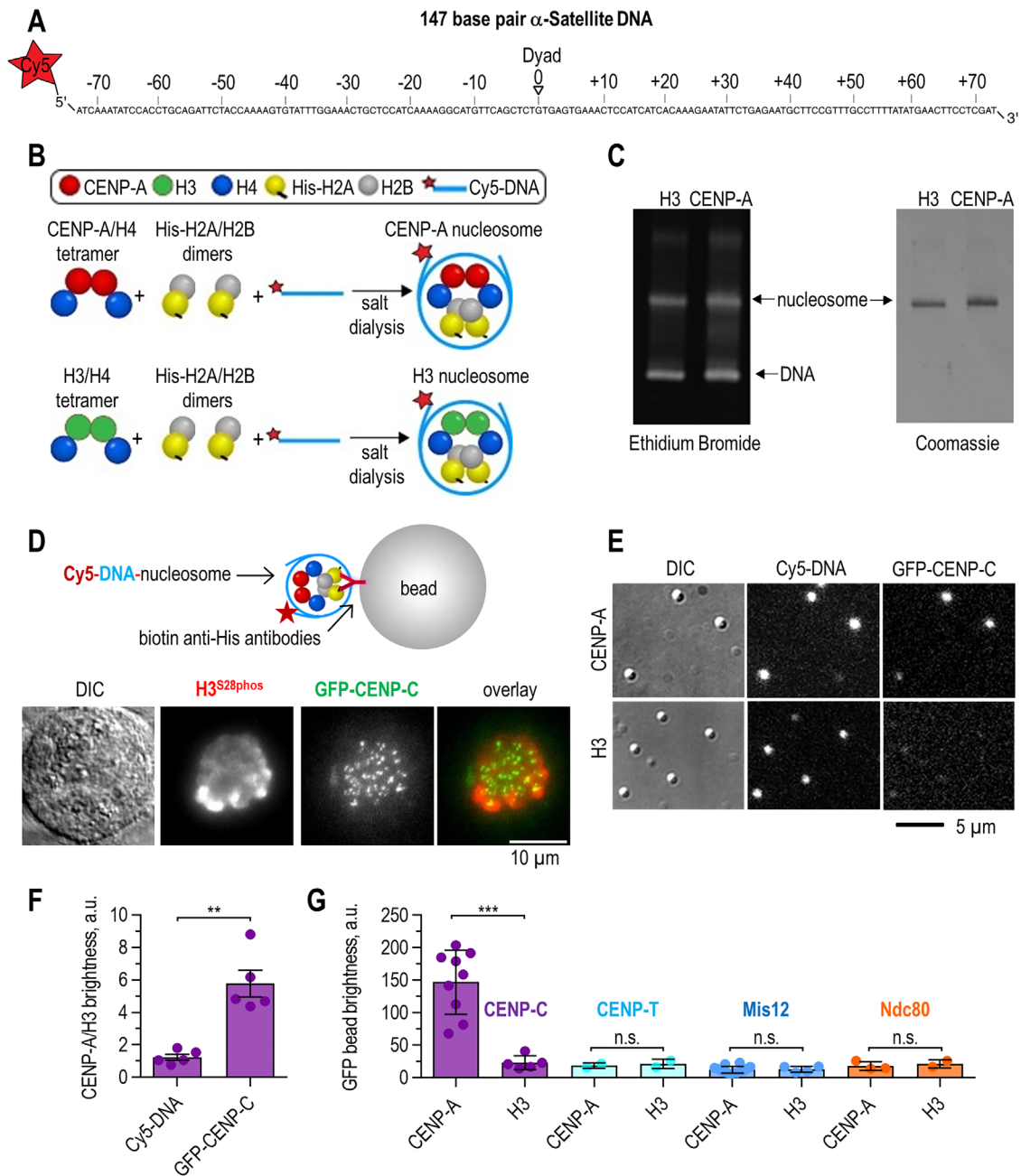


FIGURE 5: Reconstructions based on the CENP-A nucleosomes and mitotic cell extracts. (A) The DNA (147 base pairs) used in nucleosome reconstitution is a CENP-A positioning fragment from the human X-chromosome centromeric α -satellite repeat; the 5' end is labeled with Cy-5. (B) Schematic and constituents required to reconstitute nucleosomes with labeled DNA and His-H2A protein. (C) Nucleosomes prepared by gradient salt dialysis were analyzed by separation on native PAGE followed by ethidium bromide and Coomassie staining. (D) Schematic of nucleosome immobilization on beads and an example of a mitotic HeLa cell stably expressing GFP-CENP-C, fixed and stained with anti-H3^{S28phos} antibodies to visualize chromosomes. (E) Representative images of beads in DIC and fluorescent channels, showing DNA-Cy5 and GFP-CENP-C. (F) Ratio of brightness of CENP-A- vs. H3-coated beads in the Cy5 and GFP channels. The conjugation levels of different nucleosomes are similar, but only nucleosomes containing CENP-A recruit native GFP-CENP-C. Each point in panels F and G represents the average bead brightness obtained in one independent experiment; errors are SEM. *p* values were calculated by unpaired *t* test: **, *p* < 0.01; ***, *p* < 0.001, n.s., not significant. For more detailed statistics, see the Supplemental Source data. (G) Average GFP brightness of beads reflects the level of recruitment of the indicated kinetochore components to different nucleosomes. Means are shown with SD.

cells in which both copies of the endogenous CENP-C gene were tagged with yellow fluorescent protein (YFP) (Supplemental Figure 4B), indicating that these interactions can take place at physiological levels of CENP-C.

To determine the degree to which outer kinetochore components could assemble on this molecular platform, we incubated nucleosome-coated beads with extracts prepared from cells stably expressing GFP-tagged Mis12 or Ndc80. However, we observed

low GFP signal for beads coated with CENP-A or H3 nucleosomes, indicating poor Mis12 and Ndc80 recruitment (Figure 5G; Supplemental Figure 4, C and D). We then examined whether recruitment of outer kinetochore components could be enhanced by CENP-A polynucleosomes, which represent a more natural molecular environment for kinetochore assembly. We designed polynucleosome arrays containing six CENP-A nucleosomes, wrapped around 1195-base-pair DNA from human chromosome 21 α -satellite (Ohzeki *et al.*, 2002) (Supplemental Figure 5, A and B; Supplemental Materials and Methods). Beads coated with CENP-A polynucleosomes or H3 polynucleosomes as a control were incubated with cell extracts containing GFP-tagged CENP-C or Ndc80 complex. However, the binding levels by Ndc80 complexes were still low (Supplemental Figure 6, A–C). Consistently, we did not detect any increase in microtubule binding by the polynucleosome-containing beads incubated with mitotic cell extracts (Supplemental Figure 6D). Thus, native CENP-C complex bound to either CENP-A nucleosomes or their arrays cannot nucleate recruitment of outer kinetochore components from cell extracts.

Removal of the auto-inhibitory domain of Mis12 complex improves its recruitment to CENP-C but only partially

Phosphorylation of the N-terminal tail of Dsn1 subunit is a key step for kinetochore assembly via the CENP-C pathway in *Xenopus* egg extracts (Bonner *et al.*, 2019). We did not expect phosphorylation of the Dsn1 tail to be prevented in human mitotic cell extracts because they contain endogenous Aurora B kinase, and our lysis buffer included an ATP regeneration system. However, the activity of the soluble Aurora B kinase pool toward the Mis12 complex may be insufficient for robust Mis12 activation (Bonner *et al.* 2019). In *Xenopus*, *S. cerevisiae*, *Kluyveromyces lactis*, chicken, and human systems, the requirement of Mis12 phosphorylation for CENP-C binding can be bypassed by introducing the truncations or phosphomimetic substitutions at the Dsn1 N-terminus, thereby generating an autoinhibition-deficient Mis12 complex (Akiyoshi *et al.*, 2013; Kim and Yu, 2015; Rago *et al.*, 2015; Dimitrova *et al.*, 2016; Petrovic *et al.*, 2016; Hara *et al.*, 2018; Lang *et al.*, 2018; Bonner *et al.*, 2019; Hamilton *et al.*, 2020).

We generated a HeLa cell line stably expressing GFP-fused Mis12 complex in which the auto-inhibitory region at the N-terminus of the Dsn1 subunit was deleted (GFP-Dsn1- Δ 91-113) (Figure 6A). In previous studies (Kim and Yu, 2015) and in our experiments, this mutant exhibits constitutive kinetochore association, indicating that it is highly active for CENP-C binding at kinetochores of HeLa cells (Supplemental Figure 7). Extracts prepared from mitotically arrested GFP-Dsn1- Δ 91-113 cells were incubated with beads coated with either CENP-A or H3 nucleosomes (Figure 6B). There was a significant heterogeneity in GFP intensity of the beads. On average, mutant Mis12-GFP complexes were recruited to the CENP-A-containing beads more strongly than wild-type Mis12-GFP complexes (Figure 6C). However, this increase could partially be attributed to a higher level of expression of truncated protein, which resulted in a fourfold higher concentration of soluble mutant versus wild-type Mis12 complexes (Supplemental Figure 8D). A similar lack of enhanced Mis12 binding to CENP-C was seen in DLD-1 cells expressing the autoinhibition-deficient Mis12 complex with two phosphomimetic substitutions in the Dsn1 subunit (Supplemental Note 1; Supplemental Figures 9 and 10). Consistently with the lack of strong assembly activity, soluble GFP-Dsn1- Δ 91-113 complexes from mitotic extracts did not associate with native Ndc80 complexes and demonstrated relatively weak affinity for microtubules (Supplemental Note 2; Supplemental Figures 3 and 8, A and B). We conclude

that phosphoregulation of the Dsn1 tail is not the major factor limiting Mis12 binding to the CENP-A nucleosome-bound CENP-C in human cell extracts.

We investigated other prominent factors that have been implicated in enhancing kinetochore assembly reactions, but none could overcome marked inhibition of the KMN complexes recruitment in cell extracts. First, CENP-A nucleosome arrays did not differ significantly from the CENP-A mononucleosomes in promoting Mis12 recruitment to CENP-C (Supplemental Figure 6, A–C). Second, although clustering of CENP-C proteins on the bead surface led to the overall higher Mis12 binding, the efficiency of Mis12 recruitment and microtubule binding did not increase (Figure 6D). Third, we combined different molecular nucleators, such as CENP-T, CENP-C, CENP-A, and H3 nucleosomes, but these complex molecular ensembles were not sufficient to promote *de novo* assembly of microtubule-binding subcomplexes (Supplemental Note 3; Supplemental Figure 8, E and F). Thus, multiple experimental evidence points to the existence of inhibitory mechanisms that limit kinetochore assembly in mitotic cell extracts.

DISCUSSION

Inspired by previous kinetochore reconstruction studies in yeast and frog egg systems (Sorger *et al.*, 1994; Akiyoshi *et al.*, 2010; Guse *et al.*, 2011; Haase *et al.*, 2017; Lang *et al.*, 2018; Bonner *et al.*, 2019; Hamilton *et al.*, 2020), here we applied analogous strategies to investigate the assembly and microtubule-binding activities of the cytoplasmic pool of kinetochore proteins in mitotically arrested human cells (Supplemental Figure 11). Surprisingly, we found that only a few kinetochore assembly steps are permitted in human mitotic cell extracts, whereas many binding reactions are either inefficient or blocked completely (Figure 7A). This work has important implications for the mechanisms that limit the spurious formation of kinetochore assemblies in the cytoplasm of mitotic human cells, directing kinetochore assembly to centromere regions.

A subset of assembly reactions, such as those between CENP-A-containing nucleosomes and CENP-C, are permissive in human cell extracts, allowing partial reconstruction of the CENP-C-dependent kinetochore assembly pathway. However, binding of the outer kinetochore components Mis12 and Ndc80 complexes to this molecular platform is poor (Figure 5, E and F). These results are in contrast to observations in yeast, where binding to CENP-A nucleosomes activated CENP-C and promoted its binding to Mis12 (Killinger *et al.*, 2020). However, our findings are in agreement with the results of kinetochore manipulation studies in HeLa cells that used overexpression of CENP-A. When CENP-A is incorporated throughout the chromatin, it can support the recruitment of inner kinetochore proteins (CENP-C, CENP-N, and Mis18), but not the KMN components (Gascoigne *et al.*, 2011). In contrast, the KMN components can be recruited to noncentromeric CENP-A loci generated by tethering a fusion of LacI with the HJURP histone chaperone to LacO arrays (Barnhart *et al.*, 2011; Logsdon *et al.*, 2015). It is currently not known why the efficiency of outer kinetochore assembly differs among these various cellular approaches, and whether similar mechanisms could explain our *in vitro* results. The failure of KMN recruitment following CENP-A overexpression in cells could result from the limited size of soluble pools of KMN components, preventing their visible accumulation on the chromosome arms. However, as explained below, in our reconstructions the size of soluble protein pools was not a limiting factor. An alternative explanation for the different extents of KMN recruitment in various cellular approaches is that proper kinetochore assembly and maturation rely on specific cues provided by the structural and molecular

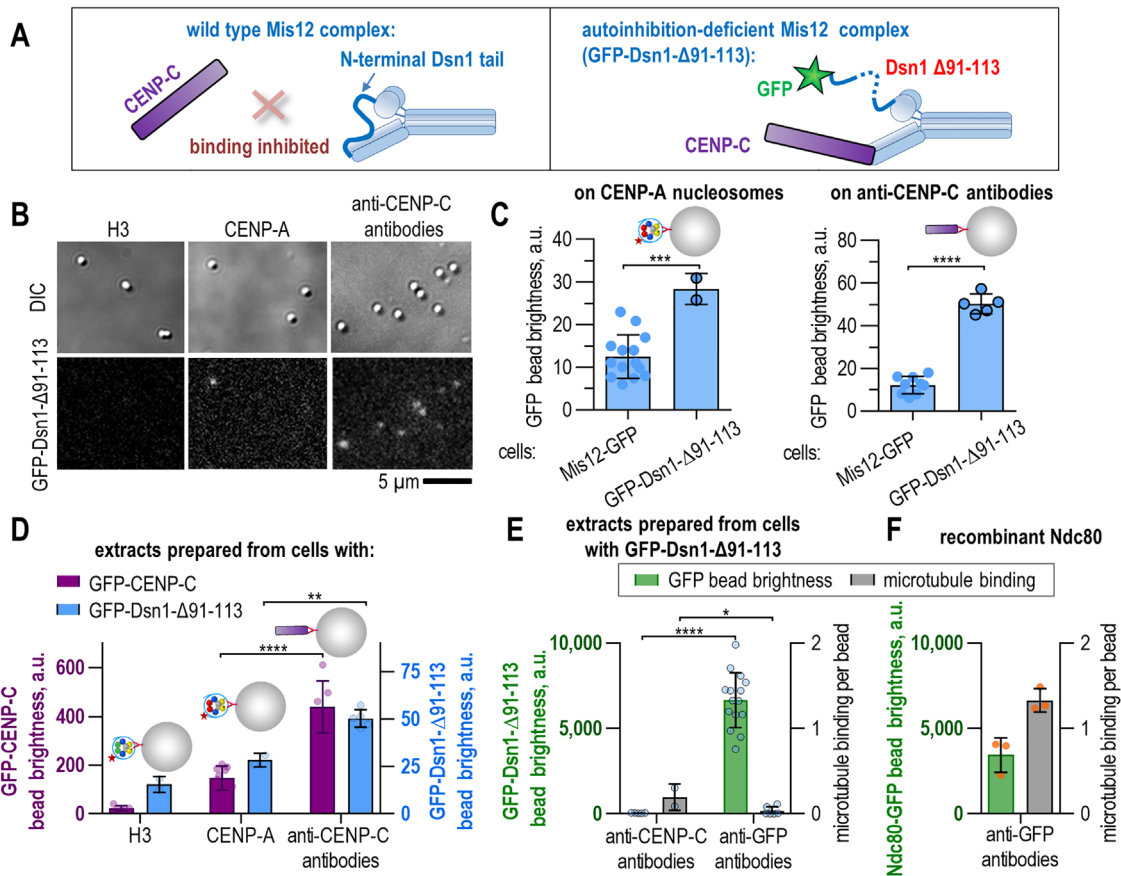


FIGURE 6: Reconstitutions using autoinhibition-deficient Mis12 complex and different modes of CENP-C recruitment to microbeads. (A) Cartoon illustrating Mis12 binding to CENP-C and Mis12 activation by a truncation within the Dsn1 N-tail. (B) Representative images of beads in the DIC and GFP channels, showing recruitment of native mutant Mis12 complexes to different nucleosomes, or to beads coated with anti-CENP-C antibodies. (C) GFP bead brightness showing recruitment of different native Mis12 complexes to beads with indicated coatings. In panels C–F, horizontal lines and column bars show means with SD, each dot represents the average result from one independent experiment. *p* values were calculated by unpaired *t* test: *, *p* < 0.05; **, *p* < 0.01; ***, *p* < 0.001; ****, *p* < 0.0001. For more detailed statistics, see the Supplemental Source data. (D) GFP-brightness of beads showing recruitment of native CENP-C and Mis12 complexes to beads with indicated coatings; data for Dsn1-Δ91-113 is the same as on panel (C), plotted here to provide side-by-side comparison with the recruitment of native CENP-C. (E) GFP-bead brightness (left axis and green columns) and the number of bead-bound microtubules (right axis and gray columns) plotted for beads with indicated compositions. Data for GFP brightness are the same as in panel (C). (F) Results of experiments similar to those in panel (E) but using recombinant Ndc80 (orange dots) in the presence of unlabeled cell extract. These data are the same as in Figure 3, C and D, and are shown here for side-by-side comparison with the recruitment activity of native kinetochore complexes.

environment at the sites with a high local density of CENP-A nucleosomes. In this case, the failure of bead-bound CENP-A nucleosomes to nucleate robust assembly of soluble kinetochore components in mitotic cell extracts could be explained by the lack of a proper milieu or an in situ regulatory modification. Our attempts to mimic this environment by using CENP-A polynucleosomes have thus far been unsuccessful. Future work is needed to identify and recapitulate the missing factors or regulatory steps.

Our attempt to reconstruct the CENP-C pathway also revealed a specific assembly step where phospho-dependent interactions between kinetochore proteins differ from the canonical views. Work in other systems identified phosphorylation of Dsn1 by Aurora B kinase as a key step that partially or completely relieves Mis12 autoinhibition, promoting its binding to kinetochore-localized CENP-C, followed by recruitment of Ndc80 complex and other outer kinetochore proteins (Yang *et al.*, 2008; Kim and Yu, 2015; Rago *et al.*, 2015; Petrovic *et al.*, 2016; Lang *et al.*, 2018; Bonner *et al.*, 2019).

Consistently, when we used mitotic cell extracts containing activated Mis12 complex (GFP-Dsn1-Δ91-113), which localizes constitutively to HeLa kinetochores, its binding to the CENP-A-coated beads was noticeably improved relative to wild-type Mis12. However, this recruitment was still disappointingly inefficient, as only one mutant Mis12 complex was recruited per six native CENP-C molecules associated with the bead-bound CENP-A nucleosomes (Figure 6D). The total level of GFP-Dsn1-Δ91-113 binding to beads was improved by increasing twofold the density of bead-bound CENP-C molecules with the help of anti-CENP-C antibodies. However, the efficiency of CENP-C-dependent recruitment did not increase, as there was only one Mis12 complex per nine CENP-C molecules (Figure 6D), strongly suggesting that this interaction is not limited by the local concentration of CENP-C. It is also not limited by the availability of soluble Mis12 complexes, as recruitment of wild-type or mutant Mis12 complexes to beads directly via anti-GFP antibodies led to a >15-fold increase in bead brightness relative to Mis12

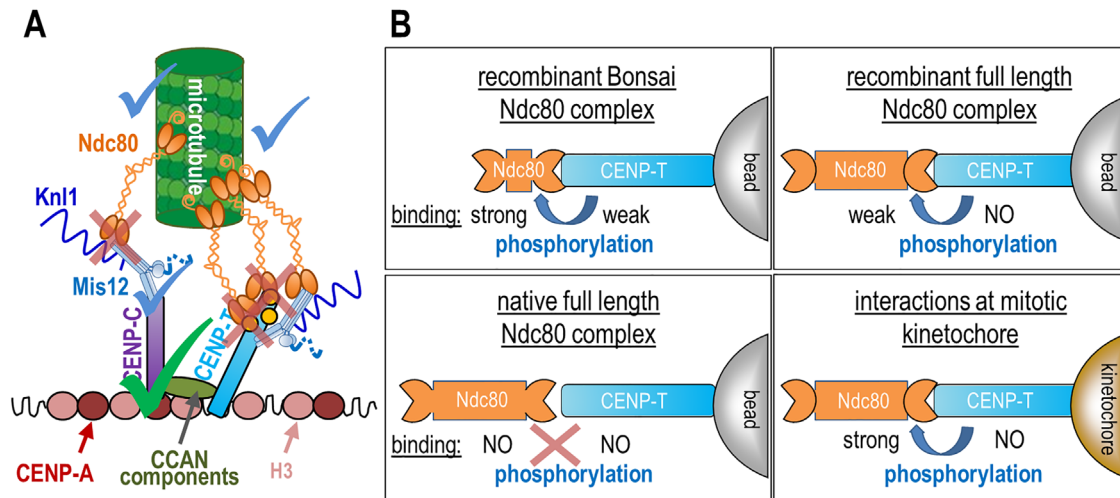


FIGURE 7: Summary of the permitted and restricted assembly steps in human cell extracts. (A) Simplified scheme indicating results from our reconstitutions: permitted assembly steps (green check mark), moderately/weakly efficient reactions (blue check mark), and restricted interactions (red crosses). Yellow circles indicate phosphomimetic substitutions in CENP-T (T11D, T27D, and T85D); dashed line in Mis12 complex indicates truncation within the Dsn1 subunit (Δ91-113). (B) Scheme illustrating binding between human CENP-T and Ndc80 complexes found for different mutants in reconstitutions in vitro and in mitotic cells. Blue arrows and red cross illustrate effect of CDK1-dependent phosphorylation on this binding. Summary scheme for native full-length Ndc80 complex in cells is based on Gascoigne *et al.* (2011), Nishino *et al.* (2013), Rago *et al.* (2015), and Huis In 't Veld *et al.* (2016).

recruitment via native CENP-C. These results strongly imply that phosphorylation of Dsn1 is not the primary factor that limits the interaction between the native Mis12 complex and CENP-C proteins in human cell extract.

The addition of centromeres to the cytosolic extracts was sufficient to induce de novo kinetochore assembly in frog and yeast systems (Supplemental Note 4). Although this does not necessarily mean that kinetochore complexes are preassembled in the cytosol, we identified an important difference between human and yeast cell extracts with regard to the Mis12-containing kinetochore complexes and their microtubule-binding activity. Only a minor fraction of soluble Mis12-containing complexes in human mitotic cell extracts bind to microtubules (Figure 2, B and C; Supplemental Figure 8, A and B), and Mis12 complexes are unable to recruit native Ndc80 complexes (Supplemental Figure 3). Consistently, human bead-bound Mis12-containing complexes have low microtubule-binding activity regardless of the mode of their recruitment to the beads: via anti-GFP antibodies, via the CENP-C bound to beads directly (with anti-CENP-C antibodies), or via bead-bound CENP-A nucleosomes (Figure 6, E and F; Supplemental Figure 8, E and F). Thus, cell extracts prepared from mitotic HeLa cells do not contain significant amounts of Mis12-containing preassembled kinetochore particles, such as those found in yeast cell extracts (Akiyoshi *et al.*, 2010).

Also unexpected was the lack of robust interactions between native CENP-T/W and Ndc80 complexes in human cell extracts, even though we readily detect interactions between the recombinant versions of these proteins (Supplemental Figure 3). Studies in different organisms found that CDK1 phosphorylation of the N-terminus of CENP-T is required for Ndc80 recruitment (Gascoigne *et al.*, 2011; Nishino *et al.*, 2013; Rago *et al.*, 2015; Huis In 't Veld *et al.*, 2016; Hara *et al.*, 2018). In agreement with this finding, we found that introducing phosphomimetic substitutions into CENP-T/W (T11D, T27D, and T85D) strengthened the interactions between recombinant CENP-T/W and different Ndc80 proteins, although recruitment of the recombinant full-length Ndc80 complex was five times weaker than that of the Ndc80 proteins with shortened stalk (Figures 4C and

7B). However, native Ndc80 complex binds very poorly to recombinant CENP-T/W complexes containing phosphomimetic substitutions, strongly implying that similarly to the Mis12 recruitment to CENP-C, phosphorylation is required but not sufficient for robust interactions between Ndc80 and CENP-T in human cells. It is possible that these interactions are promoted by other proteins that compete for CENP-T binding or somehow modify Ndc80 or CENP-T molecules. Alternatively, posttranslational modifications at the CENP-T sites that were not targeted in our mutants could play a role in CENP-T binding to Ndc80 complex.

Finally, our work also reveals a novel regulatory mechanism that limits kinetochore assembly through the auto-inhibition of full-length Ndc80 complex for CENP-T binding. Work in yeast led to a model in which full-length Ndc80 complex is bent at the hinge region, partially inhibiting the microtubule-binding activity of Ndc80 (Scarborough *et al.*, 2019). At the same time, full-length yeast Ndc80 complex is competent for binding to Mis12 complex, which then partially relieves the auto-inhibition and enhances Ndc80 binding to microtubules (Kudalkar *et al.*, 2015; Scarborough *et al.*, 2019). By contrast, human recombinant full-length Ndc80 complex binds microtubules readily, but it is inhibited for CENP-T binding (Figures 3, B and D, and 4, B and C). The auto-inhibition mechanism that prevents binding of full-length Ndc80 to CENP-T is not yet understood, but it may also include bending of the Ndc80 molecule. Indeed, the Bonsai version of the Ndc80 complex binds CENP-T well, so inhibition of full-length Ndc80 appears to depend on the coiled-coil and hinge regions that are truncated in Bonsai Ndc80. However, it remains unclear why native Ndc80 has reduced microtubule-binding affinity compared with recombinant full-length Ndc80 complex (Figures 2, B and C, and 3, B and D), even though both proteins are inhibited for CENP-T binding (Figure 4, B and C). Thus, inhibition of the Ndc80 microtubule binding in cells is not driven by the same mechanism that restricts its binding to CENP-T.

In summary, using different approaches, we found that multiple inhibitory steps prevent outer kinetochore assembly in mitotic cell extracts (Figure 7A). Based on the observed behaviors, it is difficult

to fully exclude the possibility that our experimental conditions, such as buffer composition or the mode of protein-bead conjugation, are not a sufficiently close match to the molecular milieu for kinetochore assembly reactions in live cells. However, because consistent results were obtained with different approaches and for several kinetochore components, our findings strongly suggest that the lack of active preassembled kinetochore complexes and their de novo formation in cell extracts reflects the presence of multiple physiological barriers to the assembly reactions in the cytosol of dividing cells. We hypothesize that such inhibitory mechanisms guard against spurious formation of kinetochore-like structures in cell cytoplasm, which would compete with the formation of endogenous kinetochores and interfere with chromosome motility, spindle function, or checkpoint signaling. Thus, successful assembly of human kinetochores de novo from native proteins will require reconstruction of these as-yet-unknown regulatory steps and molecular environments, paving the way to a deeper mechanistic understanding of kinetochore formation in humans.

MATERIALS AND METHODS

[Request a protocol](#) through *Bio-protocol*.

Cell lines

HeLa and DLD-1 cells were cultured in DMEM with 10% fetal bovine serum and 1% penicillin–streptomycin at 37°C in a humidified atmosphere with 5% CO₂. HeLa cells stably expressing GFP-fused kinetochore proteins (Mis12, CENP-T, Spc25, CENP-C, Nuf2, and Spc24) were kindly provided by the Lampson lab (University of Pennsylvania). The Mis12-GFP-Halo cell line was created using CRISPR-Cas9 to tag the endogenous Mis12 with GFP, as described in Zhang *et al.* (2017). Halo-GFP-CENP-T and Halo-GFP-Spc25 cell lines were created using the recombinase-mediated cassette exchange system (Zhang *et al.*, 2017). Analogous procedures were used to generate HeLa cell lines expressing Halo-GFP-CENP-C, Nuf2-GFP-Halo, and 3xHalo-GFP-Spc24. Briefly, HeLa acceptor cells were grown in six-well plates to 60–80% confluence. Cells were cotransfected with 1 µg of the corresponding plasmids and 10 ng of a Cre recombinase plasmid using Lipofectamine 2000 (Thermo Fisher Scientific). Stable cell lines were selected after 2 d of growth by the addition of 1 µg ml⁻¹ puromycin. The unlabeled cell line used in this study was the HiLo acceptor HeLa cell line (Zhang *et al.*, 2018). Additionally, we generated a clonal cell line stably expressing Mis12 complex with an N-terminal GFP-tag and truncated Dsn1 subunit (Δ91–113). This line was generated by retroviral infection of HeLa cells with a pBABE-blast-based vector, similarly to the procedure described in Gascoigne and Cheeseman (2013). DLD-1 Flp-In T-REx cells stably expressing CENP-C^{AID-EYFP/AID-EYFP} were generated as described in Fachinetti *et al.* (2015). To create the DLD-1 cell line expressing GFP-Dsn1 with two phosphomimetic substitutions (Dsn1-SD), we generated a plasmid encoding human Dsn1 with the S100D and S109D mutations. This plasmid and FLP recombinase were transfected into DLD-1-Flp-In-T-REx cells (Supplemental Figure 9A). Hygromycin selection was performed for 10 d, followed by analysis of Dsn1-SD localization in hygromycin-resistant colonies. Kinetochore localization of GFP-Dsn1 was confirmed by fluorescence microscopy (Supplemental Figure 9B). GFP-fused proteins in other cell lines also exhibited prominent kinetochore localization.

Preparation of mitotic cell extracts

Cells were arrested with 100 ng ml⁻¹ nocodazole for 14 h, at which time ~60% of cells were mitotic, as judged by differential interference contrast (DIC) and DNA visualization. Mitotic cells were har-

vested by shaking off and gentle rinsing of 15-cm tissue culture plates using a pipette. Harvested cells were pelleted and washed by centrifugations at 1000 × g in Corning phosphate-buffered saline (PBS) buffer. Cells were resuspended in 50 mM HEPES, pH 7.2, 2 mM MgCl₂, 150 mM K-glutamate, 0.1 mM EDTA, 2 mM ethylene glycol tetraacetic acid (EGTA), 10% glycerol and washed by centrifugation; cell pellets containing 0.2–0.4 × 10⁸ cells were snap-frozen and stored in liquid nitrogen. Before each experiment, one cell pellet (volume 150–300 µl) was resuspended in two volumes of ice-cold lysis buffer (50 mM HEPES, pH 7.2, 2 mM MgCl₂, 150 mM K-glutamate, 0.1 mM EDTA, 2 mM EGTA, 0.1% IGEPAL, 10% glycerol, 4 mM Mg-ATP, 2 mM dithiothreitol [DTT]) supplemented with protease inhibitors (0.2 mM 4-(2-aminoethyl)-benzenesulfonyl fluoride hydrochloride [Goldbio], 10 µg ml⁻¹ leupeptin [Roche], 10 µg ml⁻¹ pepstatin [Roche], 10 µg ml⁻¹ chymostatin [Sigma-Aldrich], Complete Mini EDTA free cocktail [Roche]), phosphatase inhibitors (100 ng ml⁻¹ microcystin-LR [Enzo Life Sciences], 1 mM sodium pyrophosphate [Sigma-Aldrich], 2 mM sodium-β-glycerophosphate [Santa Cruz Biotechnology], 100 nM sodium orthovanadate [Alfa Aesar], 5 mM sodium fluoride [Sigma-Aldrich], 120 nM okadaic acid [EMD Millipore], PhosSTOP cocktail [Roche]), and ATP regeneration system (10 mM creatine, 0.45 mg ml⁻¹ phospho-creatine kinase [Sigma-Aldrich]). During initial stages of this work, extracts were prepared using modified lysis buffer with lower ionic strength and detergent concentration (50 mM HEPES, pH 7.2, 2 mM MgCl₂, 0.1 mM EDTA, 2 mM EGTA, 0.05% IGEPAL, 10% glycerol) supplemented with Complete Mini EDTA free cocktail and PhosSTOP cocktail. In efforts to improve the activity of cell extracts, we also varied the concentration of Mg-ATP and omitted the ATP regeneration system and endonuclease. None of these conditions affected the recruitment of CENP-C, Mis12, or Ndc80 complexes to nucleosomes. In addition, there was no significant effect of these modifications on reconstitution experiments employing recombinant CENP-T/W, anti-CENP-C, or anti-GFP antibodies, so data from experiments using different buffer compositions were combined. In several experiments, cells arrested in nocodazole were also treated for 1 h before harvest with 2.5 µM ZM447439, an Aurora B inhibitor (Tocris). The inhibitor had no significant effect on the levels of CENP-C, Nuf2, or Mis12 recruitment to CENP-A nucleosomes in cell extracts (Supplemental Figure 4A). Accordingly, the data from these two conditions were combined.

For all samples, cell pellets in lysis buffer were melted on ice for 5–10 min and homogenized by pipetting. Immediately thereafter, the cells were ruptured by sonication using a Branson SFX150 Sonifier with a 3/32" microtip and the following settings: 68% power for four or five cycles consisting of 15 s ON and 30 s OFF. During the entire procedure, the microcentrifuge tubes containing the cells were kept in ice-cold water. Using DIC and GFP fluorescence imaging, we confirmed that this procedure results in efficient cell rupture without appreciable protein degradation. Subsequently, ruptured cells were treated with 1 U µl⁻¹ OmniCleave endonuclease (Lucigen) for 15 min at 37°C to release the DNA-bound protein pool. Over that time cell extracts become cloudy; to prevent pelleting of kinetochore complexes, cells were sonicated for two more cycles of 15 s ON and 30 s OFF. Finally, extract was clarified by centrifugation at 16,000 × g for 15 min at 4°C and the supernatant fraction was collected and used immediately. The concentration of kinetochore proteins was measured via GFP fluorescence, as described in Chakraborty *et al.* (2018).

Protein expression and purification

Tubulin was purified from cow brains by thermal cycling and chromatography (Miller and Wilson, 2010) and then labeled with HiLyte647

(Hyman *et al.*, 1991). Full-length wild-type CENP-T-His or phosphomimetic CENP-T-His and the untagged CENP-W genes were coexpressed in *Escherichia coli* and purified, as in Gascoigne *et al.* (2011). The phosphomimetic CENP-T mutant contains three residues mutated to aspartic acid (T11D, T27D, and T85D) in CDK phosphorylation sites. Human Bonsai Ndc80 complex containing the N-terminal fragment of Hec1 (1–286 amino acids [aa]) fused to fragment of the Spc25 (118–224 aa) with C-terminal GFP and the Nuf2 protein (1–169 aa) fused to a fragment of Spc24 (122–197 aa) was expressed and purified, as in Zaytsev *et al.* (2015). Human Broccoli Ndc80 complex containing N-terminal fragments of Hec1 (1–506 aa) and Nuf2 (1–348 aa) with GFP-tag on the C-terminus of Nuf2 was expressed and purified, as in Schmidt *et al.* (2012). Schemes of Bonsai and Broccoli Ndc80 complexes are shown in Figure 4A. The human Bonsai Ndc80-GFP construct contains the N-terminal fragment of Hec1 (1–506 aa) fused to a C-terminal fragment of the Spc25 (118–224 aa) and the Nuf2 protein (1–348 aa) fused to a C-terminal fragment of Spc24 (122–197 aa) (Wimbish *et al.*, 2020). In this construct, the GFP-tag is located on the C-terminus of the Hec1-Spc25 chain (Supplemental Figure 1). Human Bonsai Ndc80-GFP was expressed in *E. coli* and purified as in Wimbish *et al.* (2020).

The full-length GFP-fused Ndc80 complex was designed using multibac plasmids encoding Ndc80/Hec1, Nuf2, Spc24, and Spc25, which were a generous gift from Andrea Mussachio (Max Planck Institute of Molecular Physiology, Dortmund, Germany). These were used as templates for PCR with primers containing 20-base-pair overhangs for cloning into the pBig1a vector. These cassettes were subsequently cloned into the pBig1a vector by PCR using the *Swa*I cut site, as described previously (Weissmann *et al.*, 2016). Bacmid encoding the entire Ndc80 complex was generated by transforming the pBig1a-Ndc80 plasmid into DH10emBacYFP cells (Life Technologies) according to the manufacturer's protocol. Bacmid was isolated from transformed cells using isopropanol precipitation, and successful Ndc80 complex transposition was verified by selecting white colonies (lacking Bluo-Gal reactivity) and verifying the presence of all four Ndc80 subunits by PCR. Insect cells (ExpiSF9 cells; Life Technologies) were grown and maintained in ExpiSF CD medium (Life Technologies) in 250 ml culture flasks (Corning) and shaken at 125 rpm at 27°C in the dark. For the generation of baculovirus, insect cells (4 ml at 2.5×10^6 cells ml⁻¹) were transfected with 1 µg Bacmid DNA using Expifectamine 293 (Life Technologies) according to the manufacturer's instructions. After transfection, cell viability and fluorescence were monitored daily until expression was >90% (as determined by fluorescence), at which point viral stock (P0) was harvested by pelleting cells and collecting supernatant. To generate a more infectious viral stock, the P0 full-length Ndc80 viral stock was used to infect a 300 ml culture of ExpiSF9 cells at a density of 9×10^6 cells ml⁻¹. Upon falling to 50% viability and expressing full-length Ndc80 (as determined by GFP fluorescence), virus was harvested from these cells by collecting supernatant, yielding a P1 viral stock. This P1 viral stock was used to infect a culture of 300 ml cells at a density of 5×10^6 cells ml⁻¹. Following infection, cells were monitored daily for fluorescence and viability and harvested upon reaching >80% expression by centrifugation and resuspension in lysis buffer (50 mM HEPES, pH 8.5, 200 mM NaCl, 20 mM imidazole, 10% glycerol). Cells were then drop frozen and stored at –80°C. All steps following cell harvest were carried out at 4°C. The cell suspension was thawed and supplemented with protease inhibitor tablets (Roche) and 1 mM phenylmethyl sulfonyl fluoride. Cells were lysed using a microfluidic chamber at 80 psi, and cell debris was cleared by ultracentrifugation in a Beckman L8-70M rotor at 40,000 rpm for 35 min. Full-length Ndc80 complex was purified using a

three-step purification scheme consisting of affinity tag-, ion exchange-, and gel filtration-chromatography. For affinity-based purification, the cleared cell lysate containing the His-tagged Ndc80 complex was bound to a HisTrap HP column (GE Healthcare) and eluted using an isocratic elution with 300 mM imidazole. Elution fractions were pooled and diluted in low-salt lysis buffer (containing 25 mM NaCl) and then applied to a MonoQ column (GE Healthcare) for ion exchange-based purification. The Ndc80 complex was eluted from the column using a gradient elution with lysis buffer supplemented with 1 M NaCl. Protein-containing fractions were pooled and concentrated to <1 ml in a 30 kDa molecular weight cutoff filter (Millipore) for application to a size exclusion column. For size exclusion chromatography, concentrated Ndc80 complex was applied to a Superose 6 Increase 10/300 (GE) column and eluted with 1.5 column volumes of size exclusion buffer (25 mM Tris, pH 7.6, 300 mM NaCl, 1 mM EDTA, 5% glycerol). Protein-containing fractions were pooled and concentrated using a 30 kDa molecular weight cutoff filter, supplemented with 15% glycerol (for 20% final concentration), aliquoted, and drop frozen. Protein aliquots were stored at –80°C.

Preparation of antibody-coated beads

COOH-activated glass microbeads (0.5 µm; Bangs Labs) were coated with neutravidin (Thermo Fisher Scientific), as in Grishchuk *et al.* (2008). Kinetochores proteins were conjugated to these beads using antibodies that recognize specific proteins or their tags: biotinylated anti-His-tag antibodies (6 µg ml⁻¹; Qiagen, 34440), biotinylated anti-GFP antibodies (20 µg ml⁻¹; Abcam, ab6658), or biotinylated anti-rabbit antibodies (30 µg ml⁻¹; Jackson ImmunoResearch, 111-065-045). Antibodies at the indicated concentrations were incubated overnight with 4 mg ml⁻¹ neutravidin beads, blocked with 2 mM biotinylated dPEG (2.5 kDa; Quanta BioDesign), washed extensively by centrifuging three times at 2000 × *g*, and resuspended in PBS-bovine serum albumin (BSA) buffer (135 mM NaCl, 2.5 mM KCl, 10 mM Na₂HPO₄, 1.8 mM KH₂PO₄, pH 7.2, 4 mg ml⁻¹ BSA, and 2 mM DTT). Subsequently, beads with anti-rabbit antibodies were coated with 50 µg ml⁻¹ rabbit anti-CENP-T antibodies (Abcam, ab86595) or 120 µg ml⁻¹ rabbit anti-CENP-C antibodies (custom-made by Covance and affinity-purified in-house [Bassett *et al.* 2010]). A mixture of 35 µg ml⁻¹ of anti-CENP-C antibodies and 25 µg ml⁻¹ of anti-CENP-T antibodies was used to prepare beads for simultaneous recruitment of both CENP-C and CENP-T. Beads were incubated overnight with these antibodies at the indicated concentrations and washed three times. Antibody-coated beads were stored at 4°C for 7–10 d. Before use, the beads were sonicated for 10 s to reduce clumping.

Preparation of CENP-T/W-coated beads

To immobilize recombinant CENP-T/W on the beads, 90 µl of 100–125 nM CENP-T/W (wild type or phosphomimetic) in PBS-BSA buffer was mixed with 10 µl of beads coated with anti-CENP-T antibodies and incubated for 1.5–2 h at 4°C. Next, beads were washed three times, resuspended in 10 µl of the same buffer, and used immediately in bead-based reconstitution assays. We also immobilized recombinant CENP-T/W via its His-tag on the surface of the beads coated with anti-His-tag antibodies. These methods yielded similar levels of recruitment of Ndc80 and Mis12 complexes, so the resultant data were combined.

Preparation of nucleosomes and their conjugation to beads

Human CENP-A and H3 nucleosomes were prepared using the α -satellite sequence (147 base pairs) from human X-chromosome

DNA (Figure 5A), as in Sekulic and Black (2016). Briefly, Cy5-labeled 147-base-pair DNA was PCR-amplified with Cy5 custom primers in 96-well plates, followed by ResQ column purification. Subnucleosomal histone complexes were produced in *E. coli*, purified, and assembled with DNA at equimolar ratio using gradual salt dialysis followed by thermal shifting for 2 h at 55°C (Figure 5B). The formation of nucleosomes was confirmed by 5% native PAGE analysis (Figure 5C). The nucleosomes were stored at 4°C for 1–2 mo without loss of activity.

To conjugate nucleosomes to beads, anti-His-tag antibody-coated beads (10 μ l) were incubated for 1.5–2 h at 4°C with 100–200 nM of CENP-A nucleosomes, H3 nucleosomes, or a 1:1 mixture in PBS-BSA buffer supplemented with 4 mM MgCl₂. Beads were washed three times, resuspended in 10 μ l of the same buffer, and used immediately in bead-based reconstitution assays as described with other bead coatings, except that no endonuclease was added during cell extract preparation.

Bead-based reconstitution assay

For the reconstitution assay with mitotic cell extract, 90 μ l of freshly prepared extract was mixed with 10 μ l of beads coated with antibodies, recombinant CENP-T/W, or nucleosomes and incubated for 1 h at room temperature. To test the effect of the temperature, some samples were incubated at 4°C for 2–4 h. A lower temperature resulted in a similar level of kinetochore protein recruitment, so the resultant data were combined. We confirmed that under different preparation conditions cell extracts remained in mitotic state by monitoring the level of securin (Zou *et al.*, 1999) (Supplemental Figure 2). After incubation with extract, beads were washed twice in lysis buffer supplemented with protease inhibitors, phosphatase inhibitors, and an ATP regeneration system. The beads were resuspended in 25 μ l of PBS-BSA buffer supplemented with 0.1 mg ml⁻¹ glucose oxidase, 20 μ g ml⁻¹ catalase, 6 mg ml⁻¹ glucose, and 0.5% β -mercaptoethanol. In experiments with nucleosomes, all incubations were carried out in buffers supplemented with 4 mM MgCl₂ to avoid nucleosome unwrapping.

Purified recombinant proteins were used at the following concentrations, which were determined via the fluorescence microscopy approach (Chakraborty *et al.*, 2018): 100–130 nM of Bonsai Ndc80-GFP, 120–130 nM Broccoli Ndc80-GFP, 50–90 nM Bronsai Ndc80-GFP, or 100 nM full-length Ndc80 complexes. Incubation of these recombinant proteins with beads were carried out similarly in PBS-BSA; in lysis buffer supplemented with protease inhibitors, phosphatase inhibitors, and an ATP regeneration system; or in unlabeled mitotic extract prepared from control HeLa cells expressing no GFP-fused proteins.

After incubation with mitotic cell extract or recombinant proteins, the beads were washed thoroughly, and 10 μ l of beads was added on top of a coverslip, which was then covered with a glass slide to create a “wet” chamber. The chamber was sealed with VALAP (1:1:1 Vaseline/lanolin/paraffin), and images of the beads were taken immediately under the microscope in bright-field and fluorescence channels.

To quantify recruitment of the fluorescently labeled kinetochore complexes, images were analyzed using the custom-made MATLAB program “Quantification of bead brightness” (available on the Grishchuk lab website [https://www.med.upenn.edu/grishchuklab/protocols-software.html]). This program measures the integral fluorescence intensity of beads selected using bright-field images. Brightness of the same size area located near each bead is subtracted to minimize variability in background intensity. Typically, 50–100 beads were analyzed for each independent experiment,

and average fluorescence brightness was calculated. Identical quantification procedures were used throughout this study, so GFP-bead brightness can be compared directly between different panels and graphs.

Bead-based microtubule-binding assay

Stabilized fluorescent microtubules were prepared as described in Chakraborty *et al.* (2018) from a mixture of unlabeled and HiLyte647-labeled tubulin (5:1, total tubulin concentration 100 μ M) and 1 mM GMPCPP (Jena Bioscience, Jena, Germany) incubated at 37°C for 20 min. A flow chamber was prepared with a silanized coverslip and a regular glass slide using spacers made from two strips of double-sided tape, as in Chakraborty *et al.* (2018). The surface of the coverslip was activated by incubation with 22.5 μ M of biotin-BSA (Sigma-Aldrich) for 10 min, followed by incubation for 10 min with 25 μ M neutravidin. Next, beads coated with kinetochore complexes via biotinylated antibodies were diluted five times in PBS-BSA buffer, and 25 μ l of beads was introduced to the flow chamber. The chamber was incubated for 10 min to allow immobilization of beads onto the neutravidin-coated coverslip. The chamber was blocked with 1% Pluronic F-127 and 0.1 mM biotin-PEG and incubated for 15 min with GMPCPP-stabilized HiLyte647-labeled microtubules diluted 1:100 in imaging buffer (BRB80: K-PIPES, 80 mM, pH 6.9, 4 mM Mg, 1 mM EGTA, supplemented with 4 mg ml⁻¹ BSA, 2 mM DTT, 0.1 mg ml⁻¹ glucose oxidase, 20 μ g ml⁻¹ catalase, 6 mg ml⁻¹ glucose, 0.5% β -mercaptoethanol). Imaging was performed on a Nikon Eclipse Ti-E inverted microscope as described in Supplemental Materials and Methods section “Immunofluorescence of cultured cells.” Z-stacks were taken in a ± 0.25 μ m range with 0.05- μ m steps in the DIC and fluorescence channels to visualize beads and microtubules, respectively. At least four imaging fields per chamber were collected and analyzed using the Fiji software (Schindelin *et al.*, 2012). The immobilized beads and the microtubules attached to these beads were counted for each imaging field. The efficiency of microtubule binding was calculated as the total number of microtubules attached to the beads normalized against the total number of beads in each field.

TIRF microtubule-binding assay

Binding of GFP-labeled protein complexes to microtubules *in vitro* was analyzed using TIRF microscopy. Custom-made flow chambers were assembled with silanized coverslips (22 \times 22 mm), and solutions were exchanged with a peristaltic pump as in Volkov *et al.* (2014). To immobilize microtubules, the coverslip of the flow chamber was coated with anti-tubulin antibodies (Serotec, MCA2047) and blocked with 1% Pluronic F-127, and then fluorescently labeled microtubules were flowed into the chamber. Freshly prepared cell extract was diluted in imaging buffer to achieve a 2.5–3 nM concentration of the GFP-labeled component. The mixture was perfused continuously into the chamber using a peristaltic pump at 15 μ l min⁻¹ at 32°C. Experiments with purified Bronsai Ndc80-GFP complexes were carried out similarly using an aliquot of purified protein, which was thawed and centrifuged at 157,000 $\times g$ for 15 min at 4°C to remove aggregates. To account for possible stage drift, images of microtubules were taken at the beginning and end of each 30-s imaging sequence in the GFP channel. GFP images were collected in TIRF mode using stream acquisition with 100-ms exposures and the 488 nm laser at 10% power. An Andor iXon3 EMCCD camera was used with 5 \times conversion gain, 999 EM Gain Multiplier, 10 MHz readout speed, and 14-bit sensor mode. Kymographs were assembled using the Fiji software. To quantify microtubule decoration with various GFP-fused kinetochore complexes, microtubule area was

selected on the kymograph plot in the HiLyte647channel. The average GFP fluorescence intensity was calculated in this area and the area located near each microtubule. To calculate normalized GFP brightness, the background value was subtracted, and the difference was normalized against the concentration of soluble GFP-labeled protein.

ACKNOWLEDGMENTS

We are grateful to M. Lampson and H. Zhang (University of Pennsylvania) for providing HeLa cell lines stably expressing the GFP-fused kinetochore proteins CENP-C, Mis12, Nuf2, Spc24, Spc25, and CENP-T. We thank D. W. Cleveland (University of California at San Diego) for providing DLD-1 Flp-In T-REx cells stably expressing CENP-CAID-EYFP/AID-EYFP. CENP-T/W protein was purified by Florencia Rago. We are grateful to A. Musacchio (Max Planck Institute of Molecular Physiology) for providing plasmid encoding the full-length GFP-fused Ndc80 complex. We appreciate the technical assistance and insightful suggestions of Ricardo Sousa, Eirini Zoupou, Aaron (Po-Tao) Chen, and Aleksandr Maiorov. We thank J. Dawicki-McKenna and other members of the Grishchuk, Black, and Lampson labs for sharing reagents and for helpful discussions. Research reported in this publication was supported by the Pittsburgh Foundation under C. Kaufman Foundation grant KA2017-91783 to E.L.G. and B.E.B.; the National Institute of General Medical Sciences of the National Institutes of Health under award numbers R01GM098389 to E.L.G., R35GM130302 to B.E.B., R35GM130365 to J.G.D., and R35GM126930 to I.M.C.; an American Cancer Society Theory Lab Collaborative Grant (TLC-20-117-01-TLC); and the National Science Foundation (2029868) to E.L.G. and I.M.C.; and Russian Foundation for Basic Research project no. 17-00-00001 (17-24-00234).

REFERENCES

Akiyoshi B, Nelson CR, Biggins S (2013). The aurora B kinase promotes inner and outer kinetochore interactions in budding yeast. *Genetics* 194, 785–789.

Akiyoshi B, Sarangapani KK, Powers AF, Nelson CR, Reichow SL, Arellano-Santoyo H, Gonen T, Ranish JA, Asbury CL, Biggins S (2010). Tension directly stabilizes reconstituted kinetochore-microtubule attachments. *Nature* 468, 576–579.

Allu PK, Dawicki-McKenna JM, Van Eeuwen T, Slavin M, Braitbard M, Xu C, Kalisman N, Murakami K, Black BE (2019). Structure of the human core centromeric nucleosome complex. *Curr Biol* 29, 2625–2639.e2625.

Barnhart MC, Kuich PH, Stellfox ME, Ward JA, Bassett EA, Black BE, Foltz DR (2011). HJURP is a CENP-A chromatin assembly factor sufficient to form a functional de novo kinetochore. *J Cell Biol* 194, 229–243.

Bassett EA, Wood S, Salimian KJ, Ajith S, Foltz DR, Black BE (2010). Epigenetic centromere specification directs aurora B accumulation but is insufficient to efficiently correct mitotic errors. *J Cell Biol* 190, 177–185.

Bonner MK, Haase J, Swinderman J, Halas H, Miller Jenkins LM, Kelly AE (2019). Enrichment of Aurora B kinase at the inner kinetochore controls outer kinetochore assembly. *J Cell Biol* 218, 3237–3257.

Cai Y, Hossain MJ, Hériché J-K, Politi AZ, Walther N, Koch B, Wachsmuth M, Nijmeijer B, Kueblbeck M, Martinic-Kavur M, et al. (2018). Experimental and computational framework for a dynamic protein atlas of human cell division. *Nature* 561, 411–415.

Carroll CW, Milks KJ, Straight AF (2010). Dual recognition of CENP-A nucleosomes is required for centromere assembly. *J Cell Biol* 189, 1143–1155.

Chakraborty M, Tarasovets EV, Grishchuk EL (2018). In vitro reconstitution of lateral to end-on conversion of kinetochore-microtubule attachments. *Methods Cell Biol* 144, 307–327.

Chakraborty M, Tarasovets EV, Zaytsev AV, Godzi M, Figueiredo AC, Ataullakhanov FI, Grishchuk EL (2019). Microtubule end conversion mediated by motors and diffusing proteins with no intrinsic microtubule end-binding activity. *Nat Commun* 10, 1673.

Cheeseman IM (2014). The kinetochore. *Cold Spring Harb Perspect Biol* 6, a015826.

Cheeseman IM, Chappie JS, Wilson-Kubalek EM, Desai A (2006). The conserved KMN network constitutes the core microtubule-binding site of the kinetochore. *Cell* 127, 983–997.

Coy DL, Hancock WO, Wagenbach M, Howard J (1999). Kinesin's tail domain is an inhibitory regulator of the motor domain. *Nat Cell Biol* 1, 288–292.

Desai A, Deacon HW, Walczak CE, Mitchison TJ (1997). A method that allows the assembly of kinetochore components onto chromosomes condensed in clarified *Xenopus* egg extracts. *Proc Natl Acad Sci USA* 94, 12378–12383.

De Wulf P, McAinsh AD, Sorger PK (2003). Hierarchical assembly of the budding yeast kinetochore from multiple subcomplexes. *Genes Dev* 17, 2902–2921.

Dimitrova YN, Jenni S, Valverde R, Khin Y, Harrison SC (2016). Structure of the MIND complex defines a regulatory focus for yeast kinetochore assembly. *Cell* 167, 1014–1027.e1012.

Emanuele MJ, McClelland ML, Satinover DL, Stukenberg PT (2005). Measuring the stoichiometry and physical interactions between components elucidates the architecture of the vertebrate kinetochore. *Mol Biol Cell* 16, 4882–4892.

Fachinetti D, Han JS, McMahon MA, Ly P, Abdullah A, Wong AJ, Cleveland DW (2015). DNA sequence-specific binding of CENP-B enhances the fidelity of human centromere function. *Dev Cell* 33, 314–327.

Falk SJ, Guo LY, Sekulic N, Smoak EM, Mani T, Logsdon GA, Gupta K, Jansen LE, Van Duyne GD, Vinogradov SA, et al. (2015). Chromosomes. CENP-C reshapes and stabilizes CENP-A nucleosomes at the centromere. *Science* 348, 699–703.

Falk SJ, Lee J, Sekulic N, Sennett MA, Lee TH, Black BE (2016). CENP-C directs a structural transition of CENP-A nucleosomes mainly through sliding of DNA gyres. *Nat Struct Mol Biol* 23, 204–208.

Fukagawa T, Earnshaw WC (2014). The centromere: chromatin foundation for the kinetochore machinery. *Dev Cell* 30, 496–508.

Gascoigne KE, Cheeseman IM (2013). CDK-dependent phosphorylation and nuclear exclusion coordinately control kinetochore assembly state. *J Cell Biol* 201, 23–32.

Gascoigne KE, Takeuchi K, Suzuki A, Hori T, Fukagawa T, Cheeseman IM (2011). Induced ectopic kinetochore assembly bypasses the requirement for CENP-A nucleosomes. *Cell* 145, 410–422.

Grishchuk EL, Spiridonov IS, Volkov VA, Efremov A, Westermann S, Drubin D, Barnes G, Ataullakhanov FI, McIntosh JR (2008). Different assemblies of the DAM1 complex follow shortening microtubules by distinct mechanisms. *Proc Natl Acad Sci USA* 105, 6918–6923.

Gudimchuk N, Vitre B, Kim Y, Kiyatkin A, Cleveland DW, Ataullakhanov FI, Grishchuk EL (2013). Kinetochore kinesin CENP-E is a processive bi-directional tracker of dynamic microtubule tips. *Nat Cell Biol* 15, 1079–1088.

Guo LY, Allu PK, Zandarashvili L, McKinley KL, Sekulic N, Dawicki-McKenna JM, Fachinetti D, Logsdon GA, Jamiolkowski RM, Cleveland DW, et al. (2017). Centromeres are maintained by fastening CENP-A to DNA and directing an arginine anchor-dependent nucleosome transition. *Nat Commun* 8, 15775.

Gupta A, Evans RK, Koch LB, Littleton AJ, Biggins S (2018). Purification of kinetochores from the budding yeast *Saccharomyces cerevisiae*. *Methods Cell Biol* 144, 349–370.

Guse A, Carroll CW, Moree B, Fuller CJ, Straight AF (2011). In vitro centromere and kinetochore assembly on defined chromatin templates. *Nature* 477, 354–358.

Haase J, Bonner MK, Halas H, Kelly AE (2017). Distinct roles of the chromosomal passenger complex in the detection of and response to errors in kinetochore-microtubule attachment. *Dev Cell* 42, 640–654.e645.

Hamilton GE, Helgeson LA, Noland CL, Asbury CL, Dimitrova YN, Davis TN (2020). Reconstitution reveals two paths of force transmission through the kinetochore. *eLife* 9, e56582.

Hara M, Ariyoshi M, Okumura EI, Hori T, Fukagawa T (2018). Multiple phosphorylations control recruitment of the KMN network onto kinetochores. *Nat Cell Biol* 20, 1434.

Hasson D, Panchenko T, Salimian KJ, Salman MU, Sekulic N, Alonso A, Warburton PE, Black BE (2013). The octamer is the major form of CENP-A nucleosomes at human centromeres. *Nat Struct Mol Biol* 20, 687–695.

Hori T, Amano M, Suzuki A, Backer CB, Welburn JP, Dong Y, McEwen BF, Shang WH, Suzuki E, Okawa K, et al. (2008). CCAN makes multiple contacts with centromeric DNA to provide distinct pathways to the outer kinetochore. *Cell* 135, 1039–1052.

Hori T, Fukagawa T (2020). Artificial generation of centromeres and kinetochores to understand their structure and function. *Exp Cell Res* 389, 111898.

- Hori T, Shang WH, Takeuchi K, Fukagawa T (2013). The CCAN recruits CENP-A to the centromere and forms the structural core for kinetochore assembly. *J Cell Biol* 200, 45–60.
- Huis In 't Veld PJ, Jegathan S, Petrovic A, Singh P, John J, Krenn V, Weissmann F, Bange T, Musacchio A (2016). Molecular basis of outer kinetochore assembly on CENP-T. *eLife* 5, 21007.
- Hyman A, Drechsel D, Kellogg D, Salsler S, Sawin K, Steffen P, Wordeman L, Mitchison T (1991). Preparation of modified tubulins. *Methods Enzymol* 196, 478–485.
- Itzhak DN, Tyanova S, Cox J, Borner GH (2016). Global, quantitative and dynamic mapping of protein subcellular localization. *eLife* 5, 16950.
- Kato H, Jiang J, Zhou BR, Rozendaal M, Feng H, Ghirlando R, Xiao TS, Straight AF, Bai Y (2013). A conserved mechanism for centromeric nucleosome recognition by centromere protein CENP-C. *Science* 340, 1110–1113.
- Killinger K, Bohm M, Steinbach P, Hagemann G, Bluggel M, Janen K, Hohoff S, Bayer P, Herzog F, Westermann S (2020). Auto-inhibition of Mif2/CENP-C ensures centromere-dependent kinetochore assembly in budding yeast. *EMBO J* 39, e102938.
- Kim S, Yu H (2015). Multiple assembly mechanisms anchor the KMN spindle checkpoint platform at human mitotic kinetochores. *J Cell Biol* 208, 181–196.
- Krizaic I, Williams SJ, Sanchez P, Rodriguez-Corsino M, Stukenberg PT, Losada A (2015). The distinct functions of CENP-C and CENP-T/W in centromere propagation and function in *Xenopus* egg extracts. *Nucleus* 6, 133–143.
- Kudalkar EM, Scarborough EA, Umbreit NT, Zelter A, Gestaut DR, Riffle M, Johnson RS, MacCoss MJ, Asbury CL, Davis TN (2015). Regulation of outer kinetochore Ndc80 complex-based microtubule attachments by the central kinetochore Mis12/MIND complex. *Proc Natl Acad Sci USA* 112, E5583–E5589.
- Lang J, Barber A, Biggins S (2018). An assay for de novo kinetochore assembly reveals a key role for the CENP-T pathway in budding yeast. *eLife* 7, e37819.
- Logsdon GA, Barrey EJ, Bassett EA, DeNizio JE, Guo LY, Panchenko T, Dawicki-McKenna JM, Heun P, Black BE (2015). Both tails and the centromere targeting domain of CENP-A are required for centromere establishment. *J Cell Biol* 208, 521–531.
- McIntosh JR, Grishchuk EL, Morphew MK, Efremov AK, Zhudenko K, Volkov VA, Cheeseman IM, Desai A, Mastronarde DN, Ataullakhanov FI (2008). Fibrils connect microtubule tips with kinetochores: a mechanism to couple tubulin dynamics to chromosome motion. *Cell* 135, 322–333.
- McKinley KL, Cheeseman IM (2016). The molecular basis for centromere identity and function. *Nat Rev Mol Cell Biol* 17, 16–29.
- Miller HP, Wilson L (2010). Preparation of microtubule protein and purified tubulin from bovine brain by cycles of assembly and disassembly and phosphocellulose chromatography. *Methods Cell Biol* 95, 3–15.
- Musacchio A, Desai A (2017). A molecular view of kinetochore assembly and function. *Biology (Basel)* 6, 5.
- Nagpal H, Fukagawa T (2016). Kinetochore assembly and function through the cell cycle. *Chromosoma* 125, 645–659.
- Nishino T, Rago F, Hori T, Tomii K, Cheeseman IM, Fukagawa T (2013). CENP-T provides a structural platform for outer kinetochore assembly. *EMBO J* 32, 424–436.
- Nishino T, Takeuchi K, Gascoigne KE, Suzuki A, Hori T, Oyama T, Morikawa K, Cheeseman IM, Fukagawa T (2012). CENP-T-W-S-X forms a unique centromeric chromatin structure with a histone-like fold. *Cell* 148, 487–501.
- Ohzeki J, Nakano M, Okada T, Masumoto H (2002). CENP-B box is required for de novo centromere chromatin assembly on human alphoid DNA. *J Cell Biol* 159, 765–775.
- Pesenti ME, Prumbaum D, Auckland P, Smith CM, Faesen AC, Petrovic A, Erent M, Maffini S, Pentakota S, Weir JR, et al. (2018). Reconstitution of a 26-subunit human kinetochore reveals cooperative microtubule binding by CENP-OPQR and NDC80. *Mol Cell* 71, 923–939.e910.
- Petrovic A, Keller J, Liu Y, Overlack K, John J, Dimitrova YN, Jenni S, van Gerwen S, Stege P, Wohlgenuth S, et al. (2016). Structure of the MIS12 complex and molecular basis of its interaction with CENP-C at human kinetochores. *Cell* 167, 1028–1040.e1015.
- Petrovic A, Pasqualato S, Dube P, Krenn V, Santaguida S, Cittaro D, Monzani S, Massimiliano L, Keller J, Tarricone A, et al. (2010). The MIS12 complex is a protein interaction hub for outer kinetochore assembly. *J Cell Biol* 190, 835–852.
- Powers AF, Franck AD, Gestaut DR, Cooper J, Graczyk B, Wei RR, Wordeman L, Davis TN, Asbury CL (2009). The Ndc80 kinetochore complex forms load-bearing attachments to dynamic microtubule tips via biased diffusion. *Cell* 136, 865–875.
- Rago F, Gascoigne KE, Cheeseman IM (2015). Distinct organization and regulation of the outer kinetochore KMN network downstream of CENP-C and CENP-T. *Curr Biol* 25, 671–677.
- Sandall S, Severin F, McLeod IX, Yates JR 3rd, Oegema K, Hyman A, Desai A (2006). A Bir1-Sli15 complex connects centromeres to microtubules and is required to sense kinetochore tension. *Cell* 127, 1179–1191.
- Scarborough EA, Davis TN, Asbury CL (2019). Tight bending of the Ndc80 complex provides intrinsic regulation of its binding to microtubules. *eLife* 8, e44489.
- Schindelin J, Arganda-Carrera I, Frise E, Kaynig V, Longair M, Pietzsch T, Preibisch S, Rueden C, Saalfeld S, Schmid B, et al. (2012). Fiji: an open-source platform for biological-image analysis. *Nat Methods* 9, 676–682.
- Schmidt JC, Arthanari H, Boeszoromenyi A, Dashkevich NM, Wilson-Kubalek EM, Monnier N, Markus M, Oberer M, Milligan RA, Bathe M, et al. (2012). The kinetochore-bound Ska1 complex tracks depolymerizing microtubules and binds to curved protofilaments. *Dev Cell* 23, 968–980.
- Sekulic N, Black BE (2016). Preparation of recombinant centromeric nucleosomes and formation of complexes with nonhistone centromere proteins. *Methods Enzymol* 573, 67–96.
- Sorger PK, Severin FF, Hyman AA (1994). Factors required for the binding of reassembled yeast kinetochores to microtubules in vitro. *J Cell Biol* 127, 995–1008.
- Suzuki A, Badger BL, Salmon ED (2015). A quantitative description of Ndc80 complex linkage to human kinetochores. *Nat Commun* 6, 8161.
- Volkov VA, Zaytsev AV, Grishchuk EL (2014). Preparation of segmented microtubules to study motions driven by the disassembling microtubule ends. *J Vis Exp* 2014, 51150.
- Watanabe R, Hara M, Okumura EI, Herve S, Fachinetti D, Ariyoshi M, Fukagawa T (2019). CDK1-mediated CENP-C phosphorylation modulates CENP-A binding and mitotic kinetochore localization. *J Cell Biol* 218, 4042–4062.
- Weir JR, Faesen AC, Klare K, Petrovic A, Basilico F, Fischböck J, Pentakota S, Keller J, Pesenti ME, Pan D, et al. (2016). Insights from biochemical reconstitution into the architecture of human kinetochores. *Nature* 537, 249–253.
- Weissmann F, Petzold G, VanderLinden R, Huis In 't Veld PJ, Brown NG, Lampert F, Westermann S, Stark H, Schulman BA, Peters JM (2016). biG-Bac enables rapid gene assembly for the expression of large multisubunit protein complexes. *Proc Natl Acad Sci USA* 113, E2564–E2569.
- Wimbish RT, DeLuca KF, Mick JE, Himes J, Jimenez-Sanchez I, Jeyaprakash AA, DeLuca JG (2020). The Hec1/Ndc80 tail domain is required for force generation at kinetochores, but is dispensable for kinetochore-microtubule attachment formation and Ska complex recruitment. *Mol Biol Cell* 31, 1453–1473.
- Yan K, Yang J, Zhang Z, McLaughlin SH, Chang L, Fasci D, Ehrenhofer-Murray AE, Heck AJR, Barford D (2019). Structure of the inner kinetochore CCAN complex assembled onto a centromeric nucleosome. *Nature* 574, 278–282.
- Yang Y, Wu F, Ward T, Yan F, Wu Q, Wang Z, McGlothen T, Peng W, You T, Sun M, et al. (2008). Phosphorylation of HsMis13 by Aurora B kinase is essential for assembly of functional kinetochore. *J Biol Chem* 283, 26726–26736.
- Zaytsev AV, Mick JE, Maslennikov E, Nikashin B, DeLuca JG, Grishchuk EL (2015). Multisite phosphorylation of the NDC80 complex gradually tunes its microtubule-binding affinity. *Mol Biol Cell* 26, 1829–1844.
- Zhang H, Aonbangkhen C, Tarasovets EV, Ballister ER, Chenoweth DM, Lampson MA (2017). Optogenetic control of kinetochore function. *Nat Chem Biol* 13, 1096–1101.
- Zhang H, Chenoweth DM, Lampson MA (2018). Optogenetic control of mitosis with photocaged chemical dimerizers. *Methods Cell Biol* 144, 157–164.
- Zou H, McGarry TJ, Bernal T, Kirschner MW (1999). Identification of a vertebrate sister-chromatid separation inhibitor involved in transformation and tumorigenesis. *Science* 285, 418–422.